REPORT DOCUMENTATION PAGE

Form Approved OMB NO. 0704-0188

1. REPORT DATE (DD-MM-YYYY)	2. REPORT TYPE	3. DATES COVERED (From - To)
03-10-2021	Final Report	6-Apr-2017 - 28-Feb-2021

4. TITLE AND SUBTITLE
Final Report: A Switch Controlling Biomolecular Reconfigurability

5a. CONTRACT NUMBER
W911NF-17-1-0160

5b. GRANT NUMBER

5c. PROGRAM ELEMENT NUMBER
611102

6. AUTHORS

5d. PROJECT NUMBER

5e. TASK NUMBER

5f. WORK UNIT NUMBER

7. PERFORMING ORGANIZATION NAMES AND ADDRESSES
University of California - Santa Barbara
3227 Cheadle Hall
3rd floor, MC 2050
Santa Barbara, CA 93106 -2050

8. PERFORMING ORGANIZATION REPORT NUMBER

9. SPONSORING/MONITORING AGENCY NAME(S) AND ADDRESS (ES)
U.S. Army Research Office
P.O. Box 12211
Research Triangle Park, NC 27709-2211

10. SPONSOR/MONITOR'S ACRONYM(S)
ARO

11. SPONSOR/MONITOR'S REPORT NUMBER(S)
70792-LS.14

12. DISTRIBUTION AVAILIBILITY STATEMENT
Approved for public release; distribution is unlimited.

13. SUPPLEMENTARY NOTES
The views, opinions and/or findings contained in this report are those of the author(s) and should not contrued as an official Department of the Army position, policy or decision, unless so designated by other documentation.

14. ABSTRACT

15. SUBJECT TERMS

16. SECURITY CLASSIFICATION OF:			17. LIMITATION OF ABSTRACT	15. NUMBER OF PAGES	19a. NAME OF RESPONSIBLE PERSON
a. REPORT	b. ABSTRACT	c. THIS PAGE			Daniel Morse
UU	UU	UU	UU		19b. TELEPHONE NUMBER 805-893-3157

RPPR Final Report
as of 26-Oct-2021

Agency Code: 21XD

Proposal Number: 70792LS **Agreement Number: W911NF-17-1-0160**
INVESTIGATOR(S):

Name: Daniel E. Morse Ph.D.
Email: d_morse@lifesci.ucsb.edu
Phone Number: 8058933157
Principal: Y

Organization: **University of California - Santa Barbara**
Address: 3227 Cheadle Hall, Santa Barbara, CA 931062050
Country: USA
DUNS Number: 094878394 EIN: 956006145W
Report Date: 31-May-2021 Date Received: 03-Oct-2021
Final Report for Period Beginning 06-Apr-2017 and Ending 28-Feb-2021
Title: A Switch Controlling Biomolecular Reconfigurability
Begin Performance Period: 06-Apr-2017 **End Performance Period:** 28-Feb-2021
Report Term: 0-Other
Submitted By: Daniel Morse Email: d_morse@lifesci.ucsb.edu
Phone: (805) 893-3157

STEM Degrees: 5 **STEM Participants:** 5

Major Goals: The major goal of this project was to combine biophysical and genetic engineering approaches to identify the molecular mechanisms by which the reflectin protein transduces neuronal signals to the precisely calibrated finely tuned control of color and brightness of light reflected from intracellular Bragg reflectors in specialized skin cells of squids. We also proposed to develop techniques to genetically couple reflectin to other, non-tunable proteins, and demonstrate that such linkage will allow extension of tunable control to the conjugated carrier proteins.

Accomplishments: A. ABSTRACT: Reflectin A1 (henceforth referred to simply as “reflectin” unless otherwise specified) is a cationic, block copolymeric, initially disordered protein that mediates the neuronally triggered, osmotically mediated, dynamic fine-tuning of the color and brightness of light reflected from nanostructured Bragg reflectors in specialized skin cells of squids. Its structure consists of a peptide chain of ca. 350 amino acids, with 6 blocks of unique and highly conserved (essentially identical) sequence alterating with cationic linkers.

In our ARO-supported research (1-17), we discovered that progressive charge-neutralization of reflectin – either by neurotransmitter-activated phosphorylation in vivo, or by pH-titration, genetic engineering or anionic screening of the purified recombinant protein in vitro – drives its condensation, folding and hierarchical assembly to form liquid-liquid phase-separated particles of precisely calibrated size exponentially proportional to the extent of charge-neutralization. This assembly triggers the osmotic efflux of water from the Bragg lamellae, shrinking their thickness and spacing, while increasing their refractive index contrast – thus dynamically tuning the color while simultaneously increasing the intensity of the reflected light.

Our analyses suggest that reflectin’s behavior can be undersood as a consequence of its structure resembling a concatenate of alternating and opposing expansion and contraction springs: Coulombic repulsion of the cationic linkers (expansion) keeps the molecule in an extended and intrinsically disordered state until charge neutralization sufficiently opposes that repulsion, relaxing the stress on the conserved domains to allow the entropic drive encoded in their sequences to trigger condensation and secondary folding (contraction), with the resulting emergence of hydrophobic surfaces and beta structures that facilitate hierarchical assembly (11, 15). Interestingly, the precise calibration between the extent of charge-neutralization and size of assembly (with consequent calibration between the initiating signal and biological effect) depends on a rapid “dynamic arrest” of assembly (17).

Formally, this dynamic arrest of assembly is determined by the balance of weak, short-range attractive forces and strong long-range repulsive forces, as well understood for many colloidal systems (33, 34, 46). Once the reflectin assemblies have reached or exceeded a critical size (in the range of ca. 10-20 nm spherical diameter), we find they

transition to the liquid phase, as nanoscale droplets exhibiting liquid-liquid phase-separated (LLPS) behavior. Our most recent results suggest that the charge neutralization-regulated size of these droplet assemblies – and hence, the number of reflectin monomers in the assemblies - is regulated by the physical properties of the liquid state, principally including Plateau Rayleigh Instability (48), in which the size of the droplets is determined by the ratio of surface tension to charge. Thus, the precise calibration between the excitatory neuronal signal (with its resultingly proportional neutralization of reflectin) and the consequent osmotic dehydration of the Bragg lamellae, precisely tuning the color and brightness of the reflected light, are likely to be the direct result of the physics of the liquid state of the protein assemblies.

B. DETAILS:

a. Introduction:

Cephalopods such as squid and octopuses possess an optically dynamic epithelium, enabling complex camouflage and communication (18, 19). In addition to pigmentary chromatophores, these animals possess reflective cells – leucophores and iridocytes - that act as structural reflectors through the interaction of light with their sub-wavelength nanostructures (3, 4). While leucophores are broadband scatterers of white light, iridocytes reflect specifically colored, iridescent light by angle- and wavelength-dependent constructive interference from intracellular Bragg reflectors. The lamellae of these reflectors are densely filled with cationic block copolymer-like proteins called reflectins and are separated from the low refractive index extracellular fluid by regular invaginations of the cell membrane (4).

The structural reflectors of the iridocytes and leucophores of most cephalopods are static, but those in the Loliginid squid family uniquely possess reversibly tunable versions of these reflectors (13) (Figure 1A). Ultrastructural characterization of unactivated tunable iridocytes showed their intracellular lamellae to contain a heterogeneity of discontinuous ~10-20 nm nanoparticles and nanofibrils, suggesting that the cationic reflectins within the lamellae exist in a predominantly unassembled state dominated by inter-particle charge repulsion (21, 22). Upon iridocyte activation initiated by binding of the neurotransmitter acetylcholine (ACh; released from nearby nerve cells) to cell surface muscarinic receptors, a signal transduction cascade culminates in enzymatic phosphorylation of the reflectins, consequently neutralizing their cationic charge and driving assembly of the reflectins to form homogenously densely staining Bragg lamellae (21, 22, 1, 4). Measurements demonstrating the reversible efflux of D2O and its re-uptake revealed that condensation of the reflectins drives the expulsion of H2O from the membrane-bounded lamellae, simultaneously increasing the refractive index contrast between the intracellular and extracellular layers of the Bragg reflector while shrinking their thickness and spacing, thus activating reflectance and progressively tuning the color of the reflected light across the visible spectrum (2, 4, 5, 7). Proportionality of these responses to the activating neuronal signal results in the precisely calibrated tuning of reflected color (Figures 1B, C) (11, 15, 17).

Complete accomplishments and tables provided in uploaded file.

Training Opportunities: As described

Results Dissemination: As described

Honors and Awards: Nothing to Report

Protocol Activity Status:

Technology Transfer: 1. We transferred our newly developed low-voltage method for tuning folding and assembly of proteins (as a surrogate for their normal in vivo control by phosphorylation), together with a responsive protein and detailed instructions for use, to colleagues at the Army's CCDC Soldier Center at Natick, MA.

2. We provided recombinant reflectin-plasmid DNA expressing reflectin protein, a high-yield producing bacterial host stain, and detailed protocols for expression, purification and quality-control characterization of reflectin protein, all developed in our lab with ARO support, to Dr. Krystina Hess, Biotechnology Branch, CCDC-Chemical Biological Center (Aberdeen) and Dr. James Myslinski, US Army Futures Command, in assistance of their R&D Large-Scale Production of Reflectin for distribution to ARO researchers.

PARTICIPANTS:

RPPR Final Report
as of 26-Oct-2021

Participant Type: Postdoctoral (scholar, fellow or other postdoctoral position)
Participant: Robert Levenson
Person Months Worked: 15.00 **Funding Support:**
Project Contribution:
National Academy Member: N

Participant Type: Graduate Student (research assistant)
Participant: Daniel DeMartini
Person Months Worked: 6.00 **Funding Support:**
Project Contribution:
National Academy Member: N

Participant Type: Postdoctoral (scholar, fellow or other postdoctoral position)
Participant: Amitabh Ghoshal
Person Months Worked: 12.00 **Funding Support:**
Project Contribution:
National Academy Member: N

Participant Type: Graduate Student (research assistant)
Participant: Savannah Dearden
Person Months Worked: 15.00 **Funding Support:**
Project Contribution:
National Academy Member: N

Participant Type: Undergraduate Student
Participant: Colton Bracken
Person Months Worked: 15.00 **Funding Support:**
Project Contribution:
National Academy Member: N

Participant Type: Undergraduate Student
Participant: Christopher Sharma
Person Months Worked: 15.00 **Funding Support:**
Project Contribution:
National Academy Member: N

Participant Type: Undergraduate Student
Participant: Jerome Santos
Person Months Worked: 15.00 **Funding Support:**
Project Contribution:
National Academy Member: N

Participant Type: Other Professional
Participant: Brandon Malady

RPPR Final Report
as of 26-Oct-2021

Person Months Worked: 12.00 **Funding Support:**
Project Contribution:
National Academy Member: N

Participant Type: Postdoctoral (scholar, fellow or other postdoctoral position)
Participant: Esther Taxon
Person Months Worked: 4.00 **Funding Support:**
Project Contribution:
National Academy Member: N

ARTICLES:

Publication Type: Journal Article Peer Reviewed: Y **Publication Status:** 1-Published
Journal: Applied Physics Letters
Publication Identifier Type: ISSN Publication Identifier: 10.1063/1.4985758
Volume: 5 Issue: 10 First Page #: 104801
Date Submitted: 8/27/18 12:00AM Date Published: 10/1/17 2:00PM
Publication Location: Melville, New York, USA
Article Title: Molecular mechanism of reflectin's tunable biophotonic control: Opportunities and limitations for new optoelectronics
Authors: R. Levenson, D. DeMartini, D.E. Morse
Keywords: molecular mechanism reflectin tunable biophotonic optoelectronics
Abstract: Discovery that reflectin proteins fill the dynamically tunable Bragg lamellae in the reflective skin cells of certain squids has prompted efforts to design new reflectin-inspired systems for dynamic photonics. But new insights into the actual role and mechanism of action of the reflectins constrain and better define the opportunities and limitations for rationally designing optical systems with reflectin-based components. We and our colleagues have discovered that the reflectins function as a signal-controlled molecular machine, regulating an osmotic motor that tunes the thickness, spacing and refractive index of the tunable, membrane-bound Bragg lamellae in the iridocytes of the Loliginid squids. The tunable reflectin proteins, characterized by a variable number of highly conserved peptide domains interspersed by positively charged linker segments, are restricted in intra- and interchain contacts by Coulombic repulsion....
Distribution Statement: 3-Distribution authorized to U.S. Government Agencies and their contractors
Acknowledged Federal Support: **Y**

RPPR Final Report
as of 26-Oct-2021

Publication Type: Journal Article Peer Reviewed: Y **Publication Status:** 5-Submitted
Journal: Nature Communications
Publication Identifier Type: DOI Publication Identifier: 10.1101/456442
Volume: Issue: First Page #:
Date Submitted: 2/11/19 12:00AM Date Published:
Publication Location: New York, NY
Article Title: Neutralization of a Genetically Encoded Switch Followed by Dynamic Arrest Precisely Tunes Reflectin Assembly
Authors: R. Levenson, R. C. Bracken, C. Sharma, P. Kohl, Y. Li, J. Santos, C. Arata, D. E. Morse
Keywords: biomaterials, biophotonics, intrinsically disordered protein, tunable, iridescence, protein aggregation, protein assembly, protein self-assembly, protein phase separation, reflectins
Abstract: Only in Loliginid squids are the reflectins dynamically tunable, driving changes in skin color for camouflage and communication. The reflectins are block copolymers with repeated canonical domains interspersed with cationic linkers. Neurotransmitter-activated signal transduction culminates in catalytic phosphorylation of the cationic linkers, with resulting neutralization overcoming Coulombic repulsion, progressively allowing condensation and assembly of multimeric spheres of tunable size. Dynamic light scattering, transmission electron microscopy, small angle x-ray scattering, circular dichroism and fluorimetry now reveal details of assembly. We analyzed the assembly behavior of phospho-mimetic, deletion and other mutants in conjunction with pH-titration as an in vitro surrogate of phosphorylation to discover a predictive relationship between the extent of neutralization of the protein's net charge density and the size of the resulting multimeric protein condensates.
Distribution Statement: 3-Distribution authorized to U.S. Government Agencies and their contractors
Acknowledged Federal Support: **Y**

Publication Type: Journal Article Peer Reviewed: Y **Publication Status:** 1-Published
Journal: The Journal of Experimental Biology
Publication Identifier Type: DOI Publication Identifier: 10.1242/jeb.090415
Volume: 216 Issue: 19 First Page #: 3733
Date Submitted: 2/11/19 12:00AM Date Published:
Publication Location: Cambridge, UK
Article Title: Dynamic biophotonics: female squid exhibit sexually dimorphic tunable leucophores and iridocytes
Authors: D. DeMartini, R. Levenson, D.E. Morse, A. Ghoshal, E. Pandolfi, a Weaver. M Baum
Keywords: Doryteuthis opalescens, iridescence, iridophore, cephalopod, male mimicry, structural color
Abstract: We recently discovered that at least one species of Loliginind squids contains tunable leucophores – skin cells that can be switched from transparency to progressively brighter, broadband white reflectivity. These cells contain the same reflectin proteins in intracellular vesicles, that are found in Bragg lamellae in the color-tunable iridocytes. The mechanism of tunability in these two kinds of cells, activated by the neurotransmitter, acetylcholine (ACh) and mediated by the reflectin proteins, is apparently the same at the molecular level, with differences in the structures containing the reflectins resulting in different photo-physics. While Bragg reflection produces the tunable colors resulting changes in the refractive index, thickness and spacing of the Bragg lamellae, it is Mie scattering from the condensed reflectins and the pycnotic vesicles that contain them that produces the broadband white of the leucophores.
Distribution Statement: 3-Distribution authorized to U.S. Government Agencies and their contractors
Acknowledged Federal Support: **Y**

RPPR Final Report
as of 26-Oct-2021

Publication Type: Journal Article Peer Reviewed: Y **Publication Status:** 0-Other
Journal: Proceedings of the National Academy of Sciences of the United States of America
Publication Identifier Type: Publication Identifier:
Volume: Issue: First Page #:
Date Submitted: 2/11/19 12:00AM Date Published:
Publication Location: Washington, DC
Article Title: Direct observation of membrane bilayers fusion induced by relfectins, proteins in dynamically tunable reflective cells
Authors: J. Song, J. J. Santos, R. Levenson, W. Wu, D. E. Morse,
Keywords: vesicles, lipids, remodeling, fusion, protein
Abstract: Analyses by confocal fluorescence microscopy, cryo-transmission electron microscopy and dynamic light scattering reveal that the purified recombinant reflectins from a squid strongly interact with synthetic vesicles similar to cellular membranes in a multivalent manner, driving agglomeration in a ratio-dependent and saturable manner. Under specific conditions, reflectin A1 from this species, unlike reflectin C, can additionally drive fusion and tubulation of these vesicles, indicating that A1 possesses an ability to substantially alter vesicle structure. These results offer insights into the potential relationships of the reflectins with their confining Bragg lamellae, and suggest the possibility that reflectin-membrane interactions may play a role in the formation and behavior of these complex membrane nanostructures.
Distribution Statement: 3-Distribution authorized to U.S. Government Agencies and their contractors
Acknowledged Federal Support: **Y**

Publication Type: Journal Article Peer Reviewed: Y **Publication Status:** 4-Under Review
Journal: Nature Communications
Publication Identifier Type: Publication Identifier:
Volume: Issue: First Page #:
Date Submitted: 9/18/19 12:00AM Date Published:
Publication Location:
Article Title: Charge- Neutralization is the Proximate Trigger and Precise Governor of Reflectin Assembly
Authors: R. Levenson, B. Malady, T. Lee, P. Kohl, Y. Li, D. E. Morse
Keywords: biomaterials, biophotonics, intrinsically disordered protein, tunable, iridescence, protein aggregation, protein assembly, protein self-assembly, protein phase separation, reflectins
Abstract: Assembly of reflectin dynamically tunes color and brightness of light reflected from photonic nanostructures in squid skin. Neutralization by phosphorylation triggers assembly, driving osmotic dehydration of the Bragg lamellae containing reflectin to simultaneously shrink their thickness and spacing while increasing refractive index, thus tuning wavelength and brightness of reflectance. In vitro, reduction in net charge density of recombinant reflectin by pH-titration charge screening or mutation drives a finely tuned increase in size of the resulting multimeric assemblies, enabled by dynamic arrest of multimer growth and subsequent stability. This ensures reciprocally precise control of the particle number concentration of the reflectin assemblies, thereby encoding precise calibration between neuronal signaling, osmotic pressure, and the resulting optical changes. Charge regulation of reflectin assembly precisely fine-tunes a colligative property-based biological machine.
Distribution Statement: 2-Distribution Limited to U.S. Government agencies only; report contains proprietary info
Acknowledged Federal Support: **Y**

RPPR Final Report
as of 26-Oct-2021

Publication Type: Journal Article Peer Reviewed: Y **Publication Status:** 1-Published
Journal: Journal of Biological Chemistry
Publication Identifier Type: DOI Publication Identifier: 10.1074/jbc.RA119.010339
Volume: 294 Issue: 45 First Page #: 16804
Date Submitted: 8/31/20 12:00AM Date Published:
Publication Location:
Article Title: Calibration between trigger and color: Neutralization of a genetically encoded coulombic switch and dynamic arrest precisely tune reflectin assembly
Authors: R. Levenson, C Bracken, C Sharma, J. Santos, C. Arata, B Malady, D. E. Morse
Keywords: biomaterials, biophotonics, intrinsically disordered protein, tunable, iridescence, protein aggregation, protein assembly, protein self-assembly, protein phase separation, reflectins
Abstract: Reflectins are block copolymers with repeated canonical domains interspersed with cationic linkers. Neurotransmitter-activated catalytic phosphorylation of the linkers results in charge neutralization, overcoming Coulombic repulsion to progressively allow condensation, folding and assembly to form multimers of tunable size. Structural transitions of phospho-mimetic, deletion, and other mutants were analyzed by DLS, CD, TEM, AFM, SAXS and fluorimetry, using pH-titration as an in vitro surrogate of phosphorylation to discover a previously unsuspected, precisely predictive relationship between the extent of neutralization and size of the multimers that form via dynamically arrested liquid-liquid phase separated intermediates, with dynamic arrest enabling the observed fine-tuning by charge and resulting calibration between neuronal trigger and color in the squid. These results open new paths for the design of new materials with tunable properties.
Distribution Statement: 2-Distribution Limited to U.S. Government agencies only; report contains proprietary info
Acknowledged Federal Support: **Y**

Publication Type: Journal Article Peer Reviewed: Y **Publication Status:** 0-Other
Journal: Proceedings of the National Academy of Sciences of the United States of America
Publication Identifier Type: Publication Identifier:
Volume: Issue: First Page #:
Date Submitted: 9/18/19 12:00AM Date Published:
Publication Location:
Article Title: Reflectin proteins drive fusion and remodeling of synthetic membrane vesicles
Authors: J Song, J. Santos, R. Levenson, L. Velazquez, F. Zhang, D. Fygenson, W. Wu, D. E. Morse
Keywords: vesicles, lipids, remodeling, fusion, protein
Abstract: To better understand the interactions between the reflectins and the photonic membrane structures that encompass them, we analyzed the interactions of two purified reflectins with synthetic phospholipid membrane vesicles (similar in composition to cellular membranes), using confocal fluorescence microscopy, cryo-transmission electron microscopy and dynamic light scattering. The purified recombinant reflectins were found to interact with the vesicles in a multivalent manner, driving agglomeration in a ratio-dependent and saturable manner. Under specific conditions, reflectin additionally drives vesicle fusion and subsequent tabulation, in marked contrast to reflectin C. These results offer insights into the potential relationships of the reflectins with their confining Bragg lamellae, and suggest the possibility that reflectin-membrane interactions may play a role in the formation, structural maintenance and/or dynamic behavior of these biophotonically active membrane nanostructures.
Distribution Statement: 2-Distribution Limited to U.S. Government agencies only; report contains proprietary info
Acknowledged Federal Support: **Y**

RPPR Final Report
as of 26-Oct-2021

Publication Type: Journal Article Peer Reviewed: Y **Publication Status:** 1-Published
Journal: Applied Physics Letters
Publication Identifier Type: DOI Publication Identifier: 10.1063/5.0026546
Volume: 117 Issue: 22 First Page #: 220501
Date Submitted: 9/30/21 12:00AM Date Published: 11/1/20 7:00AM
Publication Location:
Article Title: Reflectin needs its intensity amplifier: Realizing the potential of tunable structural biophotonics
Authors: Daniel E. Morse, Esther Taxon
Keywords: reflection, amplifier, tunable, biophotonics
Abstract: Underwater camouflage and communication in a family of recently evolved squids are controlled, in part, by the reflectin proteins, which regulate dynamic changes in the color and intensity of light reflected from intracellular Bragg reflectors and Mie scatterers. The reflectins act as a signal transducer, precisely tuning the dimensions and refractive index of the membrane-bounded structural reflectors containing them to an extent exactly proportional to neuronal signaling. This calibration between the activating signal and the output color and intensity of reflectance is governed by the physics of the liquid state of reflectin assemblies, which osmotically fine-tune the dimensions and refractive index of the membrane-bounded structural reflectors containing them. While thin-film or genetically engineered assemblies of reflectin deliver changes in the colors of reflection approximating those of the biological system.....
Distribution Statement: 1-Approved for public release; distribution is unlimited.
Acknowledged Federal Support: **Y**

Publication Type: Journal Article Peer Reviewed: Y **Publication Status:** 1-Published
Journal: Langmuir
Publication Identifier Type: DOI Publication Identifier: 10.1021/acs.langmuir.9b03632
Volume: 36 Issue: 10 First Page #: 2673
Date Submitted: 10/1/21 12:00AM Date Published: 2/1/20 8:00AM
Publication Location:
Article Title: Reflectin Proteins Bind and Reorganize Synthetic Phospholipid Vesicles
Authors: Junyi Song, Robert Levenson, Jerome Santos, Lourdes Velazquez, Fan Zhang, Deborah Fygenson, We
Keywords: Vesicles, peptides and proteins, vesicle information, dynamic light scattering, membranes, reflectin
Abstract: The reflectin proteins have been extensively studied for their role in reflectance in cephalopods. In the recently evolved Loliginid squids, these proteins and the structural color they regulate are dynamically tunable, enhancing their effectiveness for camouflage and communication. In these species, the reflectins are found in highest concentrations within the structurally tunable, membrane enclosed, periodically stacked lamellae of subcellular Bragg reflectors and in the intracellular vesicles of specialized skin cells known as iridocytes and leuocophores, respectively. To better understand the interactions between the reflectins and the membrane structures that encompass them, we analyzed the interactions of two purified reflectins with synthetic phospholipid membrane vesicles similar in composition to cellular membranes, using confocal fluorescence microscopy and dynamic light scattering.
Distribution Statement: 1-Approved for public release; distribution is unlimited.
Acknowledged Federal Support: **Y**

RPPR Final Report
as of 26-Oct-2021

Publication Type: Journal Article Peer Reviewed: N **Publication Status:** 0-Other
Journal: bioRxiv
Publication Identifier Type: DOI Publication Identifier: 10.1101/2021.04.23.441158
Volume: Issue: First Page #:
Date Submitted: 10/1/21 12:00AM Date Published: 4/24/21 7:00AM
Publication Location:
Article Title: Protein Charge Neutralization is the Proximate Driver Dynamically Tuning a Nanoscale Bragg Reflector
Authors: Robert Levenson, Brandon Malady, Tyler Lee, Yahya Al Sabeh, Phillip Kohl, Youli Li, Daniel E. Morse
Keywords: reflectin, nanophotonics, optics, biomaterials, assembly
Abstract: Reflectin is a cationic, block copolymeric protein that mediates the dynamic fine-tuning of color and brightness of light reflected from nanostructured Bragg reflectors in iridocyte skin cells of squids. In vivo, neuronally activated phosphorylation of reflectin triggers its assembly, driving osmotic dehydration of the membrane-bounded Bragg lamellae containing the protein to simultaneously shrink the lamellar thickness and spacing while increasing its refractive index contrast, thus tuning the wavelength and increasing the brightness of reflectance. In vitro, we show that reduction in repulsive net charge of the purified, recombinant reflectin – either (for the first time) by generalized anionic screening with salt, or by pH titration - drives a finely tuned, precisely calibrated increase in size of the resulting multimeric assemblies. The calculated effects of phosphorylation in vivo are consistent with these effects observed in vitro. X-ray scattering analyses confirm the sphericity
Distribution Statement: 2-Distribution Limited to U.S. Government agencies only; report contains proprietary info
Acknowledged Federal Support: **Y**

BOOKS:

Publication Type: Book Peer Reviewed: Y **Publication Status:** 1-Published
Publication Identifier Type: DOI Publication Identifier: 10.1088/ 051001-056006
Book Edition: Volume: Publication Year: 2018 Date Received:
Publication Location: Bristol, UK
Publisher: Bioinspiration and Biomimetics
Book Title: Special Issue on Biophotonics and Biologically Inspired Photonics
Authors: D.E. Morse, S. Johnsen
Editor:
Acknowledged Federal Support: Y

Partners

,

RPPR Final Report

as of 26-Oct-2021

I certify that the information in the report is complete and accurate:
Signature: Daniel E. Morse
Signature Date: 10/3/21 9:59AM

FINAL REPORT

Grant Number: W911NF-17-1-0160

Title: A Switch Controlling Biomolecular Reconfigurability

PI: Daniel E. Morse
University of California, Santa Barbara

Program Manager: Dr. Stephanie A. McElhinny

Reporting Period: August 1, 2017 - May 31, 2020

a. **Participants:**

Robert Levenson	Postdoctoral Researcher	34 months
Daniel DeMartini	Doctoral Student	6 months
Amitabh Ghoshal	Postdoctoral Researcher	12 months
Savannah Dearden	Master's Degree Student	34 months
Colton Bracken	Undergraduate	24 months
Christopher Sharma	Undergraduate	24 months
Jerome Santos	Undergraduate	30 months
Brandon Malady	Laboratory Assistant	12 months
Esther Taxon	Postdoctoral Researcher	4 months

b.

c. **Technical Reports**:
(previously submitted. To ARO):

Levenson, R., D. DeMartini and D.E. Morse (2017). Molecular mechanism of reflectin's tunable biophotonic control: Opportunities and limitations for new optoelectronics. Applied Physics Lett. – Materials 5, 104801: 1-12 [http://dx.doi.org/10.1063/1.4985758]

Morse, D.E. and S.,Johnsen, (Eds.), 2018. Bioinspiration and Biomimetics, Special Issue on Biophotonics and Biologically Inspired Photonics, 13: [https://doi.org/10.1088/ 051001-056006]

Levenson, R. C. Bracken, C. Sharma, J. Santos, C. Arata, B. Malady and D. E. Morse, 2019. Calibration between trigger and color: Neutralization of a genetically encoded Coulombic switch and dynamic arrest precisely tune reflectin assembly. J. Biol. Chem. 294: 16804-16815. doi: 10.1074/jbc.RA119.010339

Song, J., R. Levenson, J. Santos, L. Velazquez, F. Zhang, D. Fygenson, W. Wu and D. E. Morse, 2020. Reflectin proteins bind and reorganize synthetic membrane vesicles. Langmuir 36: 2673−2682. doi: https://dx.doi.org/10.1021/acs.langmuir.9b03632

Morse, D.E. and E. Taxon. 2020. Reflectin needs its intensity amplifier: Realizing the potential of tunable structural biophotonics. Appl. Phys. Lett. 117: 22050; https://doi.org/10.1063/5.0026546

Levenson, R., B. Malady, T. Lee, Y. Al Sabeh, P. Kohl, Y. Li and D.E. Morse, 2021 Protein charge Neutralization is the proximate driver dynamically tuning a nanoscale Bragg reflector. Preprint in BioRxiv: https://doi.org/10.1101/2021.04.23.441158

d. **STEM Student/Supported Personnel Metrics for the Reporting Period**:

(i) Number of Undergraduate STEM Students:	3
(ii) Number of Graduate STEM Students	2
(iii) Number of students that received a STEM degree	5

e. **Technology transfer**:

1. We transferred our newly developed low-voltage method for tuning folding and assembly of proteins (as a surrogate for their normal in vivo control by phosphorylation), together with a responsive protein and detailed instructions for use, to colleagues at the Army's CCDC Soldier Center at Natick, MA.

2. We provided recombinant reflectin-plasmid DNA expressing reflectin protein, a high-yield producing bacterial host stain, and detailed protocols for expression, purification and quality-control characterization of reflectin protein, all developed in our lab with ARO support, to Dr. Krystina Hess, Biotechnology Branch, CCDC-Chemical Biological Center (Aberdeen) and Dr. James Myslinski, US Army Futures Command, in assistance of their R&D Large-Scale Production of Reflectin for distribution to ARO researchers.

f. SCIENTIFIC PROGRESS AND ACCOMPLISHMENTS:

1. MAJOR GOALS:

The major goal of this project was to combine biophysical and genetic engineering approaches to identify the molecular mechanisms by which the reflectin protein transduces neuronal signals to the precisely calibrated finely tuned control of color and brightness of light reflected from intracellular Bragg reflectors in specialized skin cells of squids. We also proposed to develop techniques to genetically couple reflectin to other, non-tunable proteins, and demonstrate that such linkage will allow extension of tunable control to the conjugated carrier proteins.

2. ACCOMPLISHED UNDER GOALS:

A. ABSTRACT: Reflectin A1 (henceforth referred to simply as "reflectin" unless otherwise specified) is a cationic, block copolymeric, initially disordered protein that mediates the neuronally triggered, osmotically mediated, dynamic fine-tuning of the color and brightness of light reflected from nanostructured Bragg reflectors in specialized skin cells of squids. Its structure consists of a peptide chain of ca. 350 amino acids, with 6 blocks of unique and highly conserved (essentially identical) sequence alterating with cationic linkers.

In our ARO-supported research (1-17), we discovered that progressive charge-neutralization of reflectin – either by neurotransmitter-activated phosphorylation *in vivo,* or by pH-titration, genetic engineering or anionic screening of the purified recombinant protein *in vitro* – drives its condensation, folding and hierarchical assembly to form liquid-liquid phase-separated particles of precisely calibrated size exponentially proportional to the extent of charge-neutralization. This assembly triggers the osmotic efflux of water from the Bragg lamellae, shrinking their thickness and spacing, while increasing their refractive index contrast – thus dynamically tuning the color while simultaneously increasing the intensity of the reflected light.

Our analyses suggest that reflectin's behavior can be undersood as a consequence of its structure resembling a concatenate of alternating and opposing expansion and contraction springs: Coulombic repulsion of the cationic linkers (expansion) keeps the molecule in an extended and intrinsically disordered state until charge neutralization sufficiently opposes that repulsion, relaxing the stress on the conserved domains to allow the entropic drive encoded in their sequences to trigger condensation and secondary folding (contraction), with the resulting emergence of hydrophobic surfaces and beta structures that facilitate hierarchical assembly (11, 15). *Interestingly, the precise calibration between the extent of charge-neutralization and size of assembly (with consequent calibration between the initiating signal and biological effect) depends on a rapid "dynamic arrest" of assembly (17).*

Formally, this dynamic arrest of assembly is determined by the balance of weak, short-range attractive forces and strong long-range repulsive forces, as well understood for many colloidal systems (33, 34, 46). Once the reflectin assemblies have reached or exceeded a critical size (in the range of ca. 10-20 nm spherical diameter), we find they transition to the liquid phase, as nanoscale droplets exhibiting liquid-liquid phase-separated (LLPS) behavior. Our most recent results suggest that the charge neutralization-regulated size of these droplet assemblies – and hence, the number of reflectin monomers in the assemblies - is regulated by the physical properties of the liquid state, principally including *Plateau Rayleigh Instability* (48), in which the size of the droplets is determined by the ratio of surface tension to charge. Thus, the precise calibration between the excitatory neuronal signal (with its resultingly proportional neutralization of reflectin) and the consequent osmotic dehydration of the Bragg lamellae,

precisely tuning the color and brightness of the reflected light, are likely to be the direct result of the physics of the liquid state of the protein assemblies.

B. DETAILS:

a. Introduction:

Cephalopods such as squid and octopuses possess an optically dynamic epithelium, enabling complex camouflage and communication (18, 19). In addition to pigmentary chromatophores, these animals possess reflective cells – leucophores and iridocytes - that act as structural reflectors through the interaction of light with their sub-wavelength nanostructures (3, 4). While leucophores are broadband scatterers of white light, iridocytes reflect specifically colored, iridescent light by angle- and wavelength-dependent constructive interference from intracellular Bragg reflectors. The lamellae of these reflectors are densely filled with cationic block copolymer-like proteins called reflectins and are separated from the low refractive index extracellular fluid by regular invaginations of the cell membrane (4).

The structural reflectors of the iridocytes and leucophores of most cephalopods are static, but those in the Loliginid squid family uniquely possess reversibly tunable versions of these reflectors (13) (**Figure 1A**). Ultrastructural characterization of unactivated tunable iridocytes showed their intracellular lamellae to contain a heterogeneity of discontinuous ~10-20 nm nanoparticles and nanofibrils, suggesting that the cationic reflectins within the lamellae exist in a predominantly unassembled state dominated by inter-particle charge repulsion (21, 22). Upon iridocyte activation initiated by binding of the neurotransmitter acetylcholine (ACh; released from nearby nerve cells) to cell surface muscarinic receptors, a signal transduction cascade culminates in enzymatic phosphorylation of the reflectins, consequently neutralizing their cationic charge and driving assembly of the reflectins to form homogenously densely staining Bragg lamellae (21, 22, 1, 4). Measurements demonstrating the reversible efflux of D_2O and its re-uptake revealed that condensation of the reflectins drives the expulsion of H_2O from the membrane-bounded lamellae, simultaneously increasing the refractive index contrast between the intracellular and extracellular layers of the Bragg reflector while shrinking their thickness and spacing, thus activating reflectance and progressively tuning the color of the reflected light across the visible spectrum (2, 4, 5, 7). Proportionality of these responses to the activating neuronal signal results in the precisely calibrated tuning of reflected color (**Figures 1B, C**) (11, 15, 17).

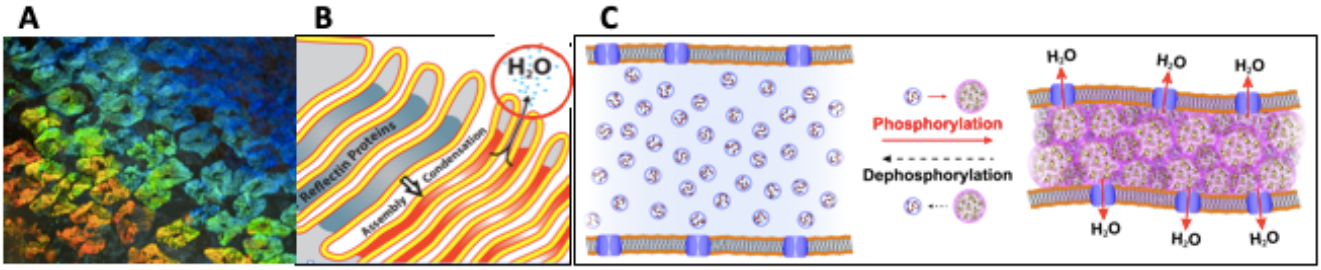

Figure 1. (A) Photomicrograph showing cascade of colors reflected from squid skin iridocytes (ca. 10 um). Activation by the neurotransmitter, ACh, induced a wave of color to ripple through the explanted skin, with cells progressively reflecting first red, then orange, yellow, green and then blue, as reflectins in the intracellular Bragg reflector lamellae condensed to osmotically shrink the thickness and spacing of the lamellae, thus activating reflectance and progressively changing its color. (10)
(B) Schematic of reflectin's mechanism of action controlling the iridocyte Bragg lamellae, as described in text. (4)
(C) Details of the molecular mechanism, by which ACh-triggered progressive phosphorylation of reflectin proportionally neutralizes its Coulombic repulsion, proportionally driving assembly, thus driving proportional osmotic dehydration of the Bragg lamella, resulting in precisely calibrated tuning of reflected color (11, 15, 17).

The role of the reflectins as a tunable driver of this biophotonic behavior has generated interest in understanding
the principles underlying their responsiveness to signal-activated phosphorylation and their resulting changes in conformation and assembly. The reflectins are essentially block copolymers, composed of highly conserved reflectin domains (RMs, for "Reflectin Motifs") interspersed with cationic linkers, as seen for the reflectins A1 and A2 of the Loliginid squid *Doryteuthis opalescens* (**Figure 2A**). The reflectins exhibit a unique amino acid composition with some heterogeneity across their sequences, being highly enriched in methionine, arginine and tyrosine residues, and possess almost no (<1%) aliphatic residues (20). The sequence architecture of the reflectins suggests that attractive interactions are likely to be primarily driven by tyrosine-aromatic (pi-pi), arginine-tyrosine (cation-pi) and methionine-tyrosine (sulfur-pi) interactions, forming a complex interaction network of both intra- and inter-strand non-covalent bonding (15, 23, 36).

We demonstrated that progressive pH-titration can be used to drive the progressive assembly of purified recombinant reflectin (11, 15, 17) as an *in vitro* surrogate for the neutralization resulting from neurotransmitter-activated phosphorylation *in vivo* (1). Analyzing the tunable reflectins and a variety of mutant derivatives, we discovered *in vitro* a predictive relationship between the extent of charge neutralization of the positively charged linker peptides and the size of the resulting assembled reflectin multimers (15) . This discovery further elucidates the mechanistic origin of the synergistic effects of reflectin neutralization on the color and brightness of light reflected *in vivo.* Mutational (deletion) analyses reveal that the "switch" controlling the neutralization-dependent structural transitions underlying tunability is not localized, but instead is spatially distributed in the multiple linkers along the reflectin's length (15).

b, Bioinformatic analyses predict the reflectins are initially disordered:

The tunable reflectins from the Loliginid squid *Doryteuthis opalescens* are essentially block-copolymeric, composed of unique and highly conserved peptide domains alternating with weakly polycationic linkers (**Figures 2A, 3)** (13, 15). Secondary structure algorithms do not predict significant alpha or beta structure, indicating that the reflectins are intrinsically disordered (11, 13, 15, 17). Comparison of *D. opalescens* reflectins A1 and A2 overall net charge and mean hydropathy with those of a collection of proteins previously analyzed for structure also indicates that the unmodified reflectins are intrinsically disordered (**Figure 2B**). Use of the FOLD-INDEX tool, which performs this same calculation using a moving window across the protein sequence, yields uniform scores across the entire reflectin A1 and A2 sequences, also indicating that the conserved domains and linkers do not vary in their drive to fold when analyzed in their unmodified, native state (15). Use of the meta-predictors PONDR-FIT and Metadisorder further support this assessment, assigning either disordered or borderline ordered scores that show no correlation with conserved domain or linker sequences (15). These bioinformatic analyses agree with previous experimental analyses of reflectin nanoparticles by x-ray scattering, circular dichroism (CD), and Fourier-transform infrared spectroscopy (FTIR), as well as the CD analyses discussed below, all indicating that unmodified reflectins are largely disordered (2, 11, 13, 28-31). Interestingly, *D. opalescens* reflectins A1 and A2 show overall greater predicted levels of intrinsic disorder than reflectins from other cephalopod species, which do not display tunable iridescence (13). This marginally greater drive of the *D. opalescens* reflectins towards disorder encoded within their sequences may play a role in enabling tunable assembly by shifting the equilibrium *in vivo* between the monomeric and assembled states, favoring disassembly in the absence of a triggering stimulus (13). In contrast, reflectins from tunable and non-tunable species show no significant differences in hydropathy (13).

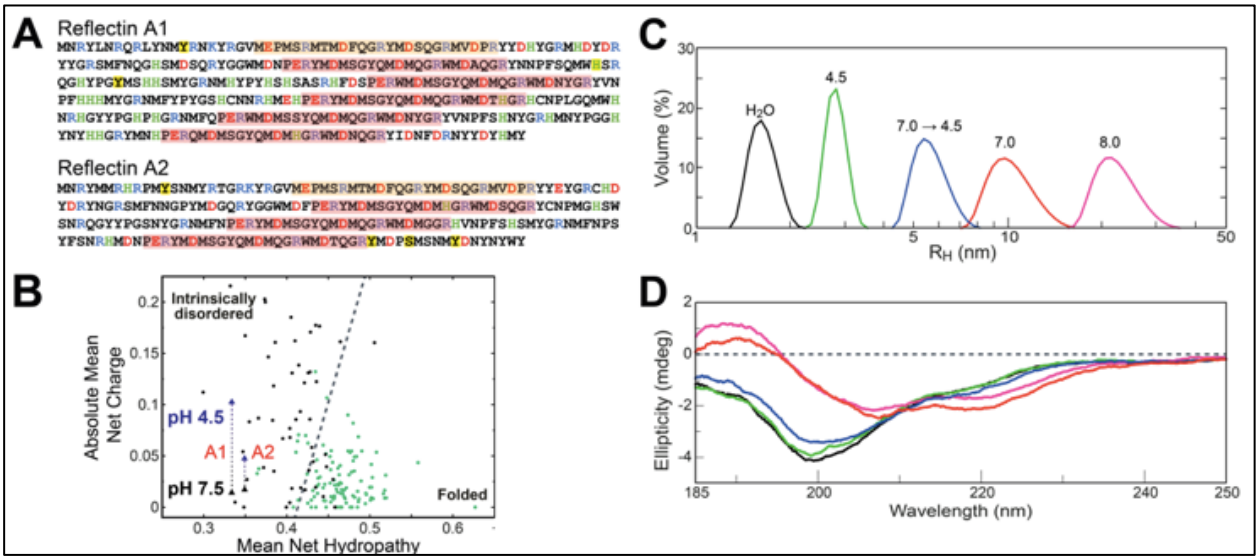

Figure 2. A) Sequences of *D. opalescens* reflectins A1 and A2. Conserved N-terminal domains are highlighted with dark yellow, other repeat domains with pale red. Histidine residues are green; other positively charged residues are blue; negatively-charged residues are bright red; phosphorylation sites are highlighted with bright yellow. **B)** Absolute mean net charge vs. hydropathy of a previously determined library of proteins (circles) and the reflectins (triangles). Yellow triangles designate mean net charge at neutral pH, where histidine residues are neutralized; red triangles designate acidic pH conditions, where histidines are presumed uniformly charged. In all other reference proteins histidines are considered neutral. Mean hydropathy calculated using the Kyte-Doolittle scale (35). **C)** DLS of A1 monomers (H_2O and pH 4.5; black and green, respectively), multimers (pH 7.0; red), and oligomers (reversed from pH 7.0 → 4.5; blue). Minority (generally <5% of total reflectin chain volume/mass) populations of substantially larger aggregates, seen previously and by other methods described in this work, are excluded from this panel for clarity (11, 15). Data show "volume distribution," which is directly proportional to the mass of reflectin, and compensates for the exponentially greater scattering intensity of larger particles. **D)** Circular dichroism spectra of A1 in monomeric, oligomeric, and multimeric states. Colors correspond to conditions as indicated for previous panel. (15)

c. Initially unstructured monomeric reflectin reversibly forms nanoparticles of well-defined size

Dynamic light scattering (DLS) of 9 μM purified recombinant reflectin A1 WT in H_2O-solubilized or acidic pH 4.5 conditions measures particles consistent with monomeric states (**Figure 2C**) (15). Dilution of H_2O-solubilized monomer into low-salt buffers at pH ≥6.5 drives reversible assembly of spherical nanoparticle multimers of tunable size, estimated to contain between tens to thousands of reflectin monomers. Sizes estimated by DLS were previously found to agree closely with those measured by TEM (11, 15). Following neutralization and assembly of the reflectins, minority populations of larger aggregates (typically <5-10% of total reflectin mass as indicated by DLS volume distributions) often were observed in addition to the majority population of predicted assemblies**,** consistent with our findings by SAXS and TEM described below and our previous observations (11). This neutralization-driven assembly can be reversed by acidification with low concentrations of acetic acid, driving disassembly to form particles with R_H values of approximately 6 nm. These particles can be cycled back to a multimeric state by dialysis into higher pH buffer, as shown previously (11).

Circular dichroism (CD) spectra of monomeric *D. opalescens* A1 WT in both H_2O-solubilized and acidic pH 4.5 conditions show strong minima near 200 nm and weak shoulders near 218 nm with both spectra, consistent with highly disordered states with a small degree of beta structure (**Figure 2D**) (15). Multimeric assembly triggered by neutralization at pH 7.0 or pH 8.0 causes a substantial change in the CD spectrum,

shifting the strong minimum and shoulder, suggesting significant structural changes during assembly. Although it is difficult to assign precise proportions of specific structures from these data, the spectra are consistent with the presence of both alpha helices and beta structures. Interestingly, the spectra of multimers at pH 7.0 and pH 8.0 are highly similar, despite the substantial difference in their sizes (R_H = 10 nm vs 20 nm, respectively). Acid-induced disassembly largely restores the CD spectrum to that of the disordered form, consistent with reversibility of reflectin conformation between the unassembled and assembled states (15).

d. Design of reflectin mutants

As summarized above, previous work showed that the tunability of *D. opalescens* reflectins is regulated by a neurotransmitter-triggered signal transduction cascade culminating in phosphorylation and consequent progressive charge-neutralization of the cationic reflectins, driving their progressive condensation and hierarchical assembly in a reversible and cyclable manner (1, 4, 11, 15). Plotting the distribution of electrostatic charge along the reflectin A1 sequence reveals a regular patterning of charges across the linkers under both acidic and neutral conditions (i.e., conditions in which the histidines are either protonated or deprotonated, respectively) (**Figure 3A**) (15). These features are generally conserved across the reflectins found in diverse cephalopods (15). We generated and analyzed a collection of *D. opalescens* reflectin A1 mutants to better analyze the effect of charge on condensation and assembly *in vitro* (**Figure 3B)** (15). A1 was chosen as the mutational platform based on its readily reproducible, tunably reversible assembly (11, 15). All mutants were expressed in bacteria and purified by methods identical to those used for the wild-type (WT), with no substantial differences from WT observed during purification. Purity of all proteins was closely similar to that of WT (11, 15).

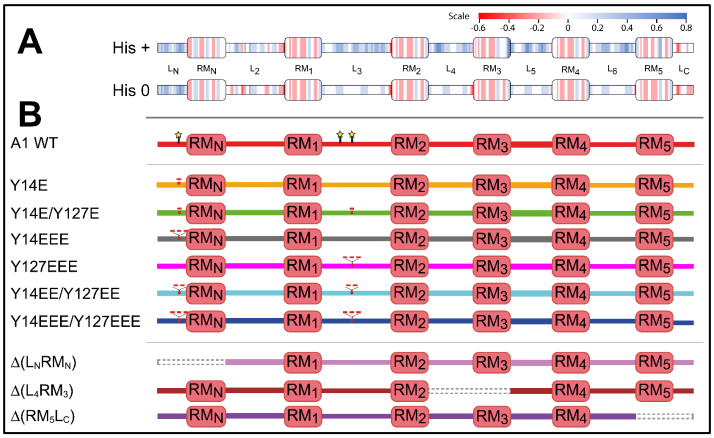

Figure 3. A) Scaled net charge across reflectin A1, in the histidine protonated (top) and histidine deprotonated (bottom) states. Color is plotted from a centered 5 residue moving window, using color key shown in figure. **B)** *D. opalescens* reflectin A1 mutationally altered proteins investigated in this work. Dotted gray lines designate deleted segments in respective mutants. In both **A** and **B**, boxes indicate conserved domains; lines indicate linkers. Stars in WT= identified phosphorylation sites. (15)

We investigated two classes of A1 mutants (15). For the first, we created a progressive series of phosphomimetic glutamate insertion mutations at two sites we previously found for *in vivo* phosphorylation (Y14 and Y127) associated with the activation of tunable iridescence in dorsal *D. opalescens* iridocytes (10). Mutants containing progressively increasing numbers of added glutamate residues allowed investigation of the incremental effects of charge neutralization on assembly, under conditions closely mimicking the effects of the physiological addition of 2 negative charges with each covalently attached phosphate. The second class of mutants consisted of deletions of conserved domain-linker segments from the N-terminal, central, or C-terminal regions of the protein. In *D. opalescens* A1,

as in other reflectins (15), the N-terminal linker is highly positive charged, whereas the more central linkers exhibit a lower but still significant net positive charge, while the C-terminus itself is negatively charged. To maintain the linker/motif balance seen in WT A-type reflectins, all deletions removed paired linker and conserved domain segments. Due to the heterogenous charge distribution across reflectin A1, each deletion therefore uniquely modified the overall charge distribution of reflectin A1.

e. Assembly size is precisely calibrated by net charge density

We analyzed the pH-dependent assembly behavior of A1 WT and mutationally altered derivatives by DLS (**Figures 4** and **5)**, transmission electron microscopy (TEM) and atomic force microscopy (AFM) (**Figure 6**) and fluorescence (15). Reliable interpretation of DLS volume distributions and R_H values requires particles to be spherical, a requirement that is justified both by the X-ray scattering discussed above, and by the TEM and AFM imaging of the WT and mutant reflectin assemblies presented below. Analyses by DLS, TEM and AFM, show that WT reflectin A1 and the phosphomimetic (glutamate addition) and deletion mutants all form spherical assemblies of low polydispersity that are morphologically similar to those previously observed for WT (11, 15). Also like WT, assemblies of the reflectin mutants with $R_H < 100$ formed rapidly (within seconds or less), while larger assembles with $R_H > 100$ nm were seen by DLS to grow more slowly (15). After their initial rapid growth, assemblies were relatively stable with time (growing no more than ca. 5-10% over several days at 25 ^oC), although particles with $R_H > 100$ nm particles were observed to settle after approximately 30 min and could not usually be recovered by resuspension. Sizes measured by DLS were reproducible, with standard deviations between experimental replicates generally < 10% when $R_H \leq 100$ nm, although larger standard deviations between replicates (up to 49%) were observed for large particle sizes ($R_H >> 100$ nm).

Significantly, reductions in reflectin's net charge through mutagenesis, mimicking the effects of neurotransmitter-activated phosphorylation *in vivo*, resulted in large, systematic and highly reproducible effects on the size of neutralization-induced assemblies. Mutationally altered reflectins with increasing numbers of additional glutamates formed progressively larger assemblies of well-defined size upon neutralization under identical conditions of pH, with this effect being enhanced at progressively higher pH (**Figure 4A-D**) (15). Both single-site single glutamate mutants, A1 Y14E and A1 Y127E, assembled to sizes in the range of A1 WT, showing that abolition of native tyrosines at those positions does not significantly perturb assembly. Further addition of negatively charged glutamates to A1 nonlinearly increased assembly size under identical pH conditions, with the effects of mutational neutralization producing exponentially greater effects as pH is increased. Interestingly, both single-site triple glutamate mutants, A1 Y14EEE and A1 Y127EEE, exhibited similarly increasing sizes across the entire range of increasing pH tested, with those sizes being intermediate to those of the double A1 Y14E/Y127E mutant (with a total of two glutamates added) and those of the A1 Y14EE/Y127EE mutant (with a total of four glutamates added), indicating a relative insensitivity to the precise location of the added negative charges. A1 Y14EEE/Y127EEE, being maximally neutralized of these glutamate mutants, resulted in the largest assemblies, with well-defined sizes up to $R_H \approx 350$ nm. All glutamate mutant assemblies were reversible by acidification with 15 mM acetic acid, pH 4.5, as previously observed for A1 WT (11).

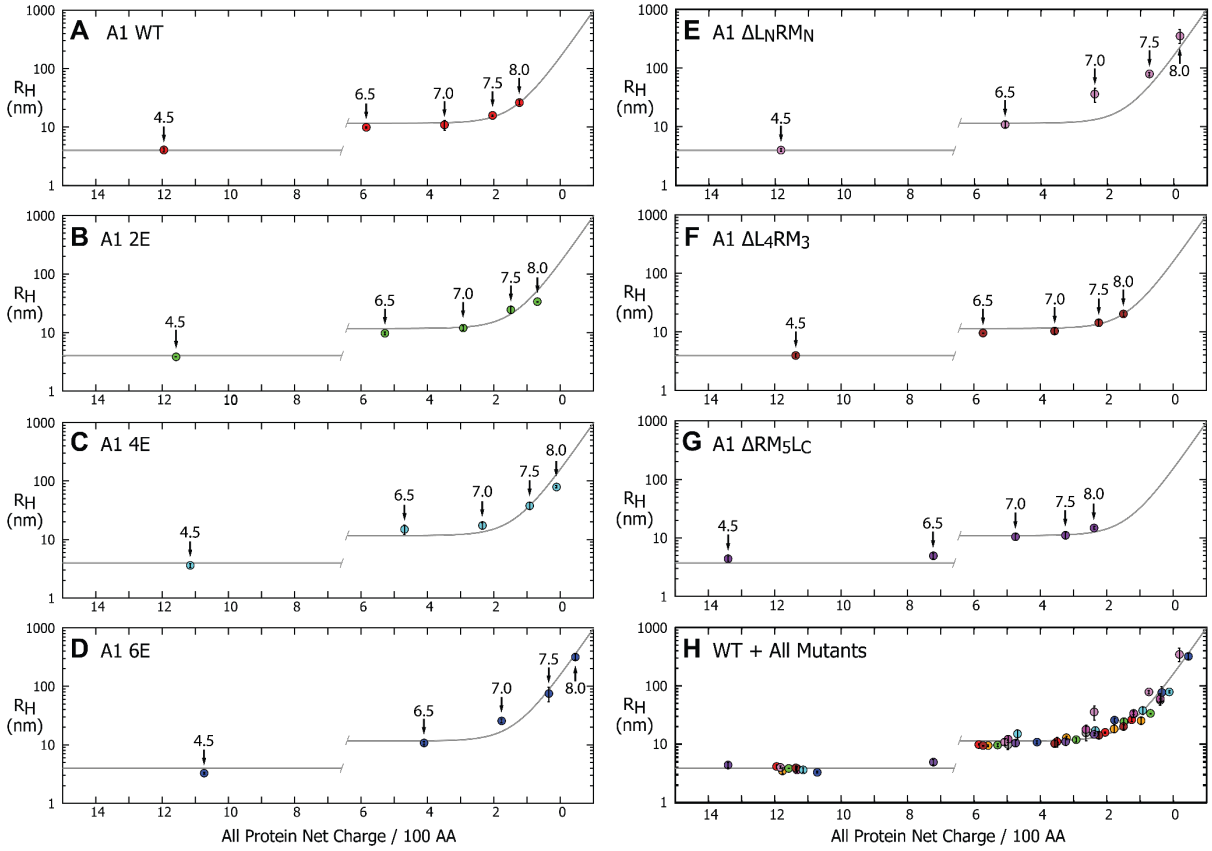

Figure 4. Experimentally determined R_H measured by DLS vs. calculated net charge density for: **A)** A1 WT. **B-D)** Selected A1 phosphomimetic mutants. **E-G)** A1 (conserved domain-linker)-deletion mutants. **H)** Data for WT and all mutants collected on a single graph. pH at each data point is labeled with arrows in panels. Discontinuous gray line is the single exponential least squares fit of all A1 data for the multimers and is plotted as flat for all monomers. Position of discontinuity between monomeric and multimeric states is estimated. Representative DLS intensity and volume data are analyzed in detail in the text and supplementary information of the publication (15). Each data point is the average of 3 replicate assembly measurements, where each assembly measurement is an average of 8 individual DLS measurements taken over the course of approximately 20 minutes immediately after sample preparation. Error bars signify ± one standard deviation between technical replicates. (15)

Deletions of conserved domain-linker pair deletions also yielded reproducible effects on assembly size upon neutralization (**Figure 4E-G**). (15). An N-terminal conserved domain-linker pair deletion (A1 $\Delta L_N RM_N$) formed particles similar in size to the maximally-neutralized phosphomimetic A1 Y14EEE/Y127EEE, while middle and C-terminal conserved domain-linker pair deletions (A1 $\Delta L_4 RM_3$ and $\Delta RM_5 L_C$, respectively) assembled to slightly decreased sizes relative to WT. Notably, A1 $\Delta RM_5 L_C$ formed $R_H \approx 4$ nm particles at pH 6.5 of likely monomeric form, (**Figure 4G**), similar to pH 4.5 conditions for WT and other mutants, and unlike the multimers normally observed at this pH. Interestingly, deletion mutants showed inconsistent reversal upon acidification with 15 mM acetic acid, pH 4.5, with oligomers only being intermittently detectable by DLS (data not shown).

f. It's the net charge density of the cationic linkers that precisely determines reflectin assembly size:

Strikingly, we found that the 30 min assembly sizes of the WT and all mutants from both classes fall on the same plot when graphed as a function the net charge density calculated for each protein. (**Figure 4**, particularly **H**) (15). Our calculation of net charge density assumed invariant sidechain pK_a's for N-

terminal, C-terminal, internal residues, and 6.5 for the histidine pK_a (11, 32). Spatial distributions of charge, calculated protein net charge and linear net charge density as a function of pH were analyzed in detail for A1 WT and the mutants discussed here. (15). An apparent discontinuity is observable between monomeric A1 at high net charge densities (typically acidic, acetate-buffered conditions), and the formation of multimers of tunable size. This suggests that a discrete neutralization threshold must be passed to trigger *D. opalescens* reflectin assembly, after which the predictive exponential relationship between net charge density and reflectin assembly size is revealed.

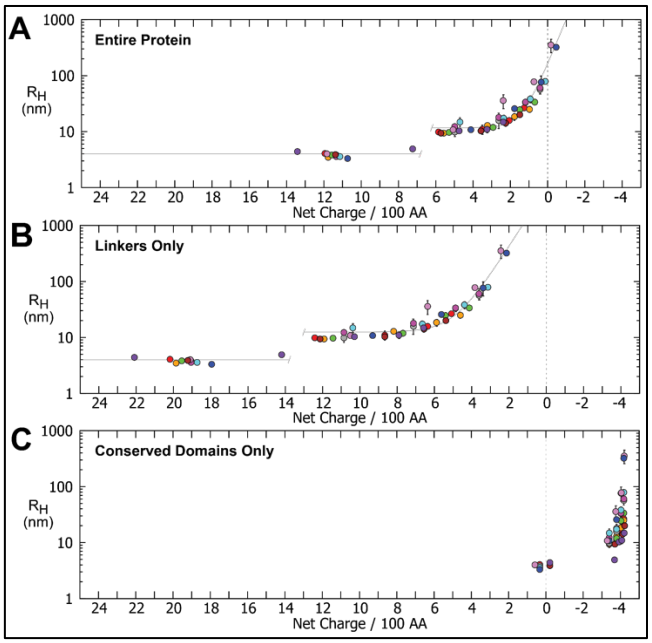

Figure 5. Experimentally measured R_H vs net charge density calculated for each entire protein or its conserved domains or linkers, for A1 WT and mutants at different pH values. Colors correspond to specific mutants as in **Figures 2 & 3**. Each data point is the average of 3 replicate assembly measurements, where each assembly measurement is an average of 8 individual DLS measurements of a sample, measured continuously, immediately after assembly. Error bars signify ± one standard deviation between averages of replicates. Gray lines are exponential fits to all multimer data in **A** and **B**, respectively**. (A)** R_H as a function of net charge density calculated for entire A1 WT and mutant proteins. (Data from **Figure 4** replotted for this comparison.) **(B)** R_H as a function of net charge density calculated only for the linkers of A1 WT and mutants. **(C)** R_H as a function of net charge density calculated only for the conserved domains (both RM_N and $RM_\#$s) of A1 WT and mutants. (15)

Decomposition of theses sequences into their component linker and domain segments shows that the net charge density of the conserved domains is poorly predictive of assembly size, while the net charge density of the linkers yields a predictive relationship with measured particle size similar to that observed for the entire protein (**Figure 5A-C**) (15). We thus conclude that the neutralization-sensitive "switch" resides in the linkers, which function like a sensor in this respect. Because reflectin assembly size appears insensitive to both the location (cf. above) and the means of charge-neutralization (whether through progressive glutamate addition, deletion, or pH titration), the switch therefore appears to be distributed among the spatially segregated linkers. These results, as illustrated in **Figures 4-5** (15), all are consistent with the behavior of a charge-stabilized colloidal system (33, 34).

Although we have shown that increases in ionic strength can drive reflectin assembly (11) by anionic charge screening (17; cf. section *h* below), the analyses reported above (15) all were conducted at low

buffer concentrations (5 mM) to minimize changes in ionic strength with pH, and comparable results were observed with MES, MOPS, and Tris buffers, with pK_a values ranging from 6.1 to 8.0. We subsequently extended these analyses to pH values as low as 4.5 (using low concentration acetate buffers) (17) with no significant differences from those shown above, indicating the absence of any large specific buffer effects. Further, the large progressive increase in assembly size of the reflectins observed as a function of added glutamate residues, all at the same value of pH, demonstrates that the assembly size differences observed between the mutants at the same pH cannot be explained by any change in ionic strength, but instead are well-predicted solely by each protein's net charge density (**Figures 4** and **5**) (15).

This precise relationship between charge density and size has a profound, direct bearing on the physiological mechanism by which reflectin controls biophotonic behavior: Because the size of the reflectin multimers is directly and inversely proportional to the *number-concentration of reflectin particles* within their membrane-bounded compartment, the charge vs. size relationship directly controls the osmotic pressure within that compartment, and thus precisely controls the osmotic dehydration of that compartment - driving the observed changes in the wavelength and intensity of the reflected light (4). The resulting dependence of this colligative property – osmotic pressure – on the extent of phosphorylation of reflectin thus ensures a precisely calibrated relationship between the neuronal delivery of ACh and the resulting color and brightness of the iridocyte. [Two other mechanisms contribute to the signal-dependent dehydration of the Bragg lamellae: "dewatering" of the reflectin molecules by steric exclusion resulting from the induced folding and hierarchical assembly of the protein, and the Gibbs-Donnan re-equilibration resulting from the similar steric displacement of some of the protein's neutralizing small counterions, transmembrane migration of these ions to maintain electrical neutrality, and the consequent movement of water to equalize osmotic pressure (4). Both mechanisms would operate in strict proportionality to the extent of assembly as well.]

g. Characterization by electron microscopy, atomic force microscopy, and fluorescence

TEM analyses confirm that the reflectin A1 WT and mutants form assemblies of spheroidal morphology and relatively low polydispersity, with sizes measured by TEM agreeing well with those determined by DLS and SAXS (**Figure 6A-E)** (15). Similarity between A1 WT and A1 Y14E confirms that tyrosine mutagenesis itself does not generate aberrant assemblies. Particle size analysis from the TEMs of A1 WT and A1 Y14EEE/Y127EEE TEM assemblies show similar magnitudes of size variation (A1 WT polydispersity = 9%; A1 Y14EEE/Y127EEE polydispersity = 16%) (15). Imaging of the N-terminal deletion $\Delta L_N RM_N$ shows that it also assembles to form spheres consistent in size with the results from DLS. Close correspondence in assembly sizes measured in the hydrated state by DLS and upon drying on TEM grids suggests that the assemblies are stable and likely to have low water content and internal dynamics, since they do not destructively shrink or collapse upon drying following application to the grid or exposure to vacuum in the electron microscope. Some larger assemblies, while appearing round in isolation, show distortions in morphology when packed into clusters, indicating that they are deformable (**Figure 6F**). Examination of air-dried reflectin particles by atomic force microscopy confirmed the highly symmetrical and smooth morphology of the reflectin assemblies (**Figure 6G, H)**. Air-dried particles showed signs of flattening vertically with concomitant lateral expansion on the glass surface, demonstrating the same deformable nature observed by TEM for packed particles.

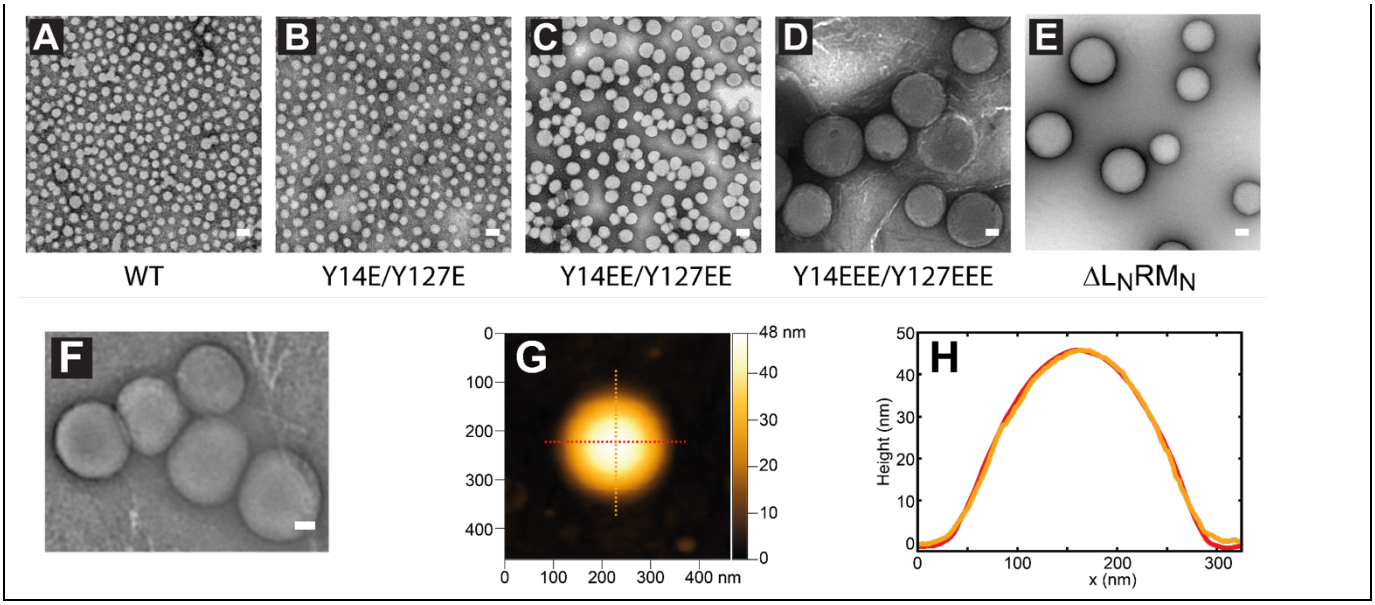

Figure 6 A-E) Transmission electron microscopy (TEM) images of A1 WT and glutamate mutants in 5 mM MOPS, pH 7.5. Scale bar = 50 nm. All TEM images in A-E have not been post-processed. Assemblies measured by DLS before application to the EM grids were: **A)** A1 WT; DLS R_H = 25 nm. **B)** A1 Y14E / Y127E; DLS R_H = 35 nm. **C)** A1 Y14EE / Y127EE; DLS R_H = 55 nm. **D)** A1 Y14EEE / Y127EEE; DLS R_H = 100 nm. **E)** A1 $\Delta L_N RM_N$; DLS R_H = 77 nm. **F)** Cluster of A1 Y14EEE / Y127EEE particles, demonstrating deformation. Image was processed using a digital bandpass filter to enhance contrast[20]. **G)** Atomic force microscope image of an A1 $\Delta L_N RM_N$ multimeric particle assembled in 5 mM MOPS, pH 7.5. **H)** Height profiles of portions of the A1 $\Delta L_N RM_N$ particle shown in previous panel, as indicated. (15)

The spheroidal and highly smooth appearance of the assemblies, particularly marked for larger assemblies such A1 Y14EEE/Y127EEE and $\Delta L_N RM_N$, strongly suggests that a liquid-like phase transition occurs during assembly. However, the observed stability of these assemblies over time and their stability after drying suggest that such a liquid-like phase possesses high interfacial energy and/or may rapidly gel in a reversible manner, although the deformable viscoelastic behavior of the large particles indicates that they are not entirely solidified.

Reflectin A1 is strongly UV-fluorescent, as it contains 10 tryptophans, 7 of which are in highly conserved positions. Tryptophan fluorescence of the various phosphomimetic mutant nanoparticulate assemblies varied with charge neutralization-driven size in a manner indistinguishable from that of WT (11, 15), demonstrating that the substitution mutations produced no significant changes in internal structure observable by this method.

h. As predicted, anionic screening is another in vitro surrogate for neutralization by phosphorylation:

We recently characterized the drive of reflectin A1 assembly by ionic screening (17), as seen in **Figure 7**, below. Results demonstrate that assembly of reflectin is driven by anionic screening of its positive charges, resulting in an effective neutralization of electrostatic repulsion that is similar to, and interacts with, the effect of pH-titration. For these experiments, purified reflectin A1 was first extensively equilibrated by dialysis into 25 mM sodium acetate
buffers at pH 4.0, 4.5, and 5.0. Dilution into the corresponding buffers containing varying concentrations of NaCl then triggered the appearance of turbidity (measured as absorbance at 350 nm) at pH-dependent salt concentration thresholds, indicating assembly, with salt concentration thresholds decreasing as pH is increased (**Figure 7A**).

Figure 7. A) Turbidity (A_{350}) of reflectin A1 solutions in 25 mM sodium acetate as a function of pH and NaCl concentration. **B)** Percent of soluble protein remaining in the supernatant after centrifugation of samples in A, relative to parallel controls with no salt. **C)** Sizes of majority populations of assembled reflectin assemblies, as measured by DLS. Each data point is an average of 40 min continuous DLS measurement (see Methods). **D-E)** Comparison of NaCl- and $CaCl_2$-induced assembly at pH 5.0, as a function of **D)** salt concentration and **E)** Cl^- anion concentration. **F)** Reflectin A1 assembly as a function of pH and NaCl concentration. Point sizes are scaled to particle size as measured by DLS. For this panel, all particles with R_H > 7.5 nm are considered assembled. From (17).

Centrifugation analyses confirmed that turbidity was due to the formation of precipitable protein assemblies (**Figure 7B**). Virtually all of the reflectin was removed by centrifugation of precipitate at higher salt concentrations and pH, demonstrating assembly of the bulk population in accord with the turbidimetric data. Measurement of these samples by DLS confirmed assembly above the threshold salt

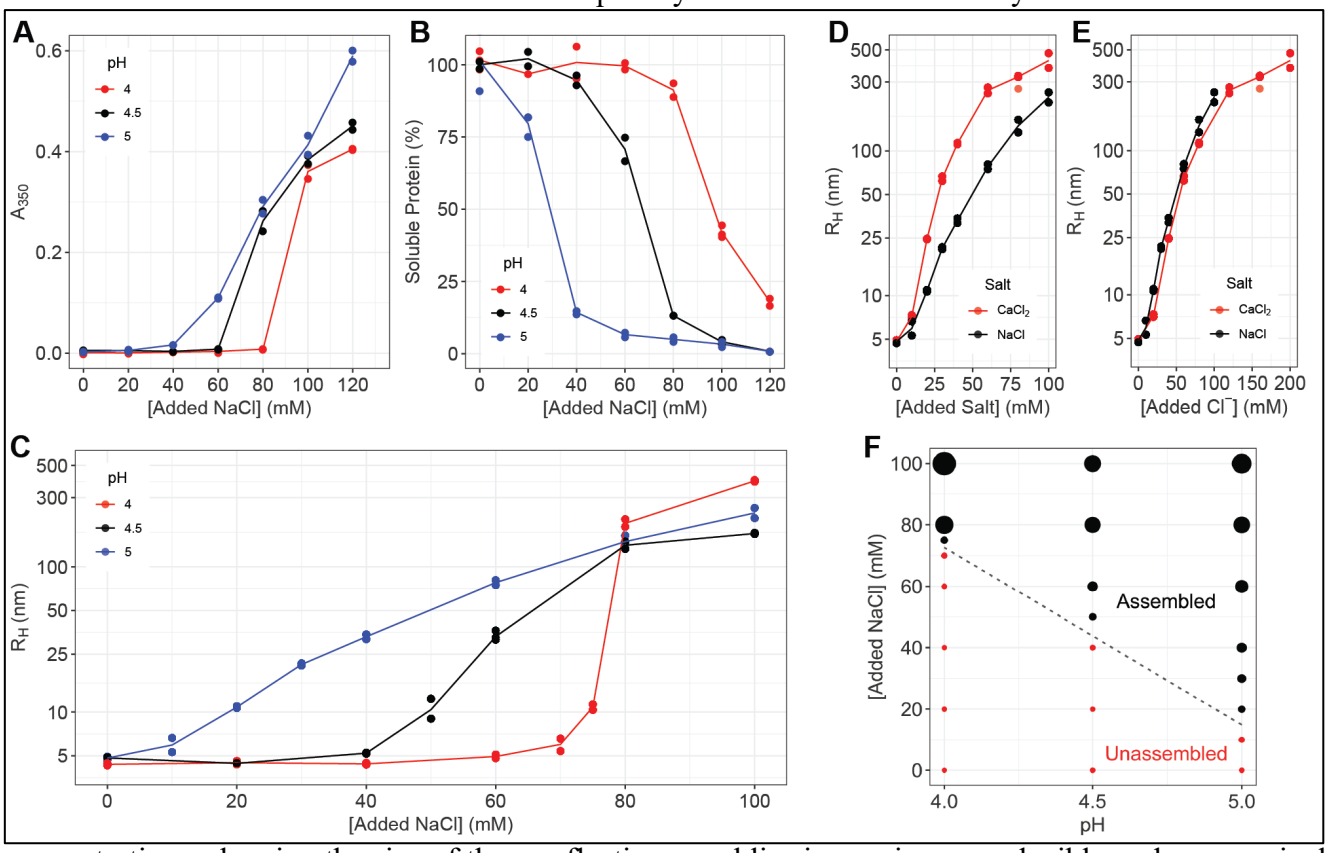

concentrations, showing the size of these reflectin assemblies increasing reproducibly and progressively with salt concentration (**Figure 7C**). These salt-driven assemblies of tunable size consisted of single majority populations as judged by DLS, with minority populations of larger particle sizes occasionally observed at lower salt concentrations. The majority populations were stable over ≥40 min (not shown), suggesting that they undergo dynamic arrest similar to that undergone by assemblies formed through pH-neutralization (cf. below). Below the salt concentration thresholds for assembly, DLS shows a majority population of stable particles of R_H = 4-5 nm, indicating the stability of the unstructured monomers under these conditions. In contrast, parallel analyses of bovine serum albumin (BSA; not shown) under identical buffer conditions showed no aggregation or assembly at all values of pH and salt concentration tested.

Significantly, twice as much monovalent NaCl is required to drive the same extent of reflectin assembly as driven by divalent $CaCl_2$ (**Figures 7D, E**), showing unequivocally that it the increasing concentration of the anion (Cl^-) that is driving assembly, by progressively screening (effectively neutralizing) the effect of reflectin's excess positive charges.

Plotting of assembly size as a function of both pH and NaCl concentration shows that the effects of charge screening and pH are interdependent, with both the salt concentration threshold and range for tunable

assembly varying systematically with pH (**Figure 7F**). The progressively lower threshold concentration for assembly at progressively higher pH is readily explained by the progressive neutralization of the protein with increasing pH, thus reducing the requirement for neutralization by charge-screening. TEM analyses (not shown) of negatively stained reflectin A1 at pH 5.0 confirm the formation of assemblies with spherical morphologies exhibiting progressively larger sizes with progressively higher salt concentrations, consistent with assemblies formed by pH-neutralized reflectin A1 wildtype and mutants (11, 15).

i. X-ray scattering and EPR confirm and extend results of dynamic light scattering, TEM and computational modelling:

Synchrotron small angle X-ray scattering (SAXS) data collected from reflectin samples in a pH-neutralized, multimeric state show characteristic features of sphere-like particles (**Figure 8)** (17). The broad peaks observed fit closely to the form factor scattering arising from the Fourier Transform of a solid sphere. The data fit closely to a model (solid line) consisting of a group of randomly dispersed solid spheres, with an average radius = 23.2 ± 3.0 nm. The fit of the data to this model is remarkably faithful except at very low Q range, where deviation can be explained by the presence of a small number of larger aggregates that were not included in the model. Details of methods and calculations were presented (17). The average radius measured by SAXS agrees well with the R_H (20 nm) measured by DLS for the same sample, and the observed polydispersity (ca. 13%) is consistent with previous estimates by DLS and TEM (11, 15). Samples prepared under different conditions exhibited a similar low polydispersity, with calculated spherical radii also closely consistent with the R_H values measured by DLS.

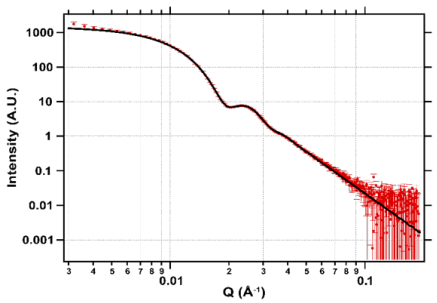

Figure 8. Synchrotron SAXS data for reflectin A1 multimers (4 mg/mL) in 15 mM MOPS, pH 7.5, after subtraction of buffer background. The data were fit to a spheroid model using SAXS modelling package IRENA, yielding an average particle radius of 23.2 nm + s.d. = 3.0 nm. DLS indicates the same sample to have R_H = 20 nm. From (17).

Recent extension of our X-ray analyses to wide-angle X-ray scattering (WAXS; **Figure 9**) reveals convincing evidence that progressive beta-sheet stacking accompanies the progressive assembly of reflectin with increasing pH, as evidenced by the emerging peak corresponding to ca. 10 A^o spacing characteristic of the beta-sheet (71).

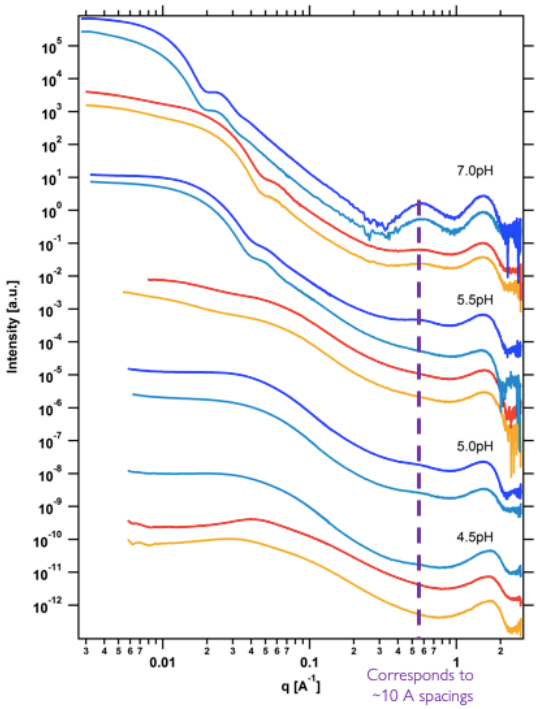

Figure 9. WAXS analyses reveal progressively increasing beta-stacking – indicated by the emerging peak at ca. 10 Aº spacing - with progressive assembly of reflectin from pH 4.5 (bottom set of traces) to pH 7.0 (top set). Each set of traces shows progressively higher reflectin concentrations, from orange to dark blue, corresponding to the range from 0.1to 10 micromolar reflectin.

EPR analyses also reveal reflectin's assembly-dependent growth of beta-sheet structure (**Figure 10**). Reflectin A1 contains cysteine residues at positions199 and 232; accordingly, we genetically replaced each, separately, with glycine, enabling us then to covalently couple the sulfur-linked spin-label, MTSL, to either the remaining 199 or 232 cysteine, yielding the corresponding two different, pure, singly spin-labeled proteins (**Figure 10, top**). EPR analyses of both as a function of pH-dependent assembly showed similar results; results for the C199-MTSL reflectin are seen in **Figure 10, bottom.** The strong J-coupling exhibited by the reflectin assemblies (ca. 27 and 67 nm diam.; pH 7 and 8, respectively), indicative of beta-sheet structure, is absent from the EPR signature of monomer (pH 4.5).

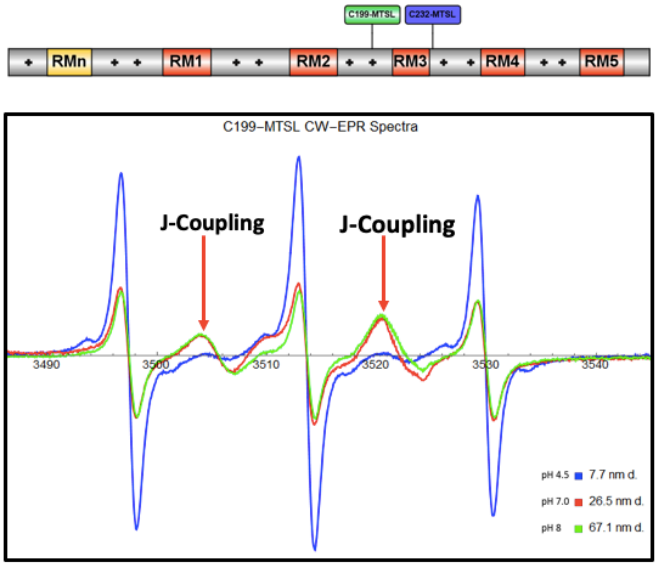

Figure 10. (top) Diagram of reflectin A1, showing conserved domains and cationic linkers to scale, with positions of the single-labeled MTSL-cysteines 199 (green) and 232 (blue).

(bottom) EPR spectra of the C100-MTSL reflectin at pH 4.5 red trace), pH 7 (blue trace) and pH 8 (green trace). These samples were analyzed by DLS and shown to have d_H values of 7.7, 26.5 and 67.1 nm, respectively.

These WAXS and EPR findings are consistent with our earlier prediction from quantitative simulations that reflectin's conserved domains have a strong potential to form amphiphilic beta structures (15), and with earlier, WAXS analyses from our lab (2) and Prof. Gorodetsky's (30) showing the emergence of beta structure with reflectin assembly.

j. Reflectin assemblies are stabilized by dynamic arrest:

Figure 11 shows the rapid dynamic arrest of growth and stabilization of reflectin assemblies. Incremental additions of reflectin monomer added successively to a buffered solution at pH 7.5 do not progressively augment the size of the initially formed multimers, but instead assemble independently upon each new addition, forming new assemblies of approximately constant size as measured by DLS (**Figure 11A**). The total particle scattering signal, a function of both particle size and concentration, increases linearly with new incremental additions of protein, showing that each newly added aliquot of reflectin does not substantially aggregate with the previously added population or precipitate (**Figure 11B**). This also is seen by comparison of changes in the intensity and volume distributions as a function of the incremental additions (**Figure 11C-D**). Significantly, the constancy of sizes indicated in the volume distribution (**Figure 11D**) confirms that the majority of reflectin monomers independently assemble to the same predetermined size upon each new addition to the same solution at fixed pH. We have noted several features of the reflectin sequence, especially including an unusually high frequency and exceptionally regular spacing of potential arginine-tyrosine cation-pi linkages, predisposing reflectin to rapidly form a network of extensive, non-covalent (intra- and inter-chain) cross-links that may contribute to such dynamic arrest (11, 15, 17). Reflectin also contains an unusually high content of tyrosine (aromatic) residues spaced with remarkably regular periodicity across the entire protein (11, 15, 17), a feature recently identified as a strong determinant of extensive pi-pi cross-linking and liquid phase behavior (36). These also may contribute to the dynamic arrest we observe.

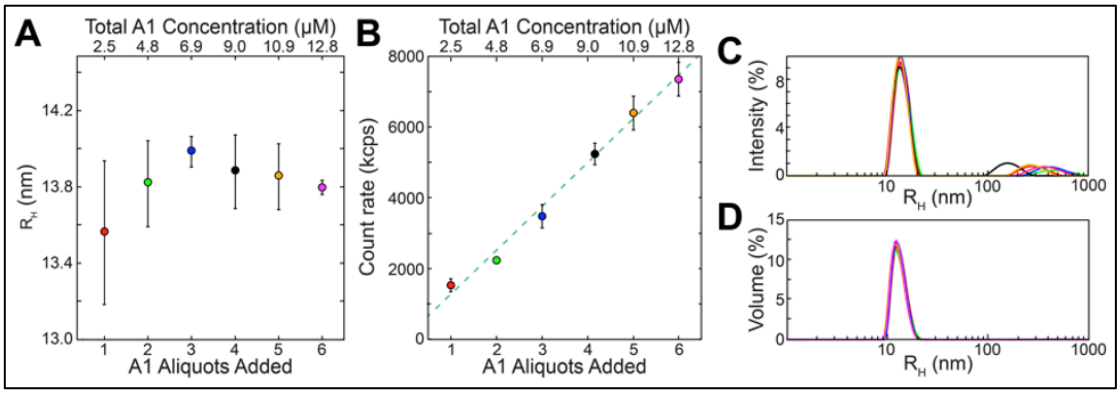

Figure 11. Assemblies of reflectin are dynamically arrested and stable, as seen in these results of incremental additions of reflectin A1 monomers to the same 5 mM MOPS, pH 7.5 (neutralizing, assembly-driving) solution. **A)** Reflectin assembly sizes (measured as the predominant DLS volume distributions; cf. Methods) as a function of monomer aliquots added. **B)** Total scattering count rate as a function of monomer aliquots added (bottom x axis) and cumulative concentration (top x axis). Each point in A-B is the average of 3 replicate experiments, in each of which every aliquot addition was analyzed by 3 individual DLS measurements; error bars signify ± one S.D. between averages of replicates. Samples showed no significant variation over time following each aliquot addition, consistent with our previous results (11, 15). Representative Intensity **(C)** and Volume **(D)** distributions observed after addition of the 6th aliquot of monomer, with results after each aliquot shown in a different color. From (17).

k. Reflectin assemblies ≥ 10-20 nm diameter are liquid:

Our most recent experiments have confirmed and extended our previous finding (15) indicating that the reflectins are liquid-liquid phase-separated nanodroplets. First suggested by our observation that the assemblies large enough to be well-resolved by TEM (i.e., ≥ 10-20 nm diameter) are spherical (11), liquidity has now been confirmed by fluorimetric analyses, taking advantage of the larger assemblies afforded by anionic screening (17; cf. 48) that make confocal microscopic analyses possible. Two lines of evidence now unequivocally confirm liquidity of these assemblies: FRAP (fluorescence recovery after photo-bleaching) and merger of fluorescein-labeled reflectin droplets (**Figures 12, 13**); a third

observation (exchange of fluorescein- and rhodamine-labeled reflectins in droplets) further supports that conclusion.

For these analyses, one of the two cysteine residues in the reflectin A1 sequence was genetically replaced with glycine, and the sulfhydryl side-chain of the remaining cysteine then used to covalently and site-specifically couple an appropriately modified fluorescein (that fluoresces green).

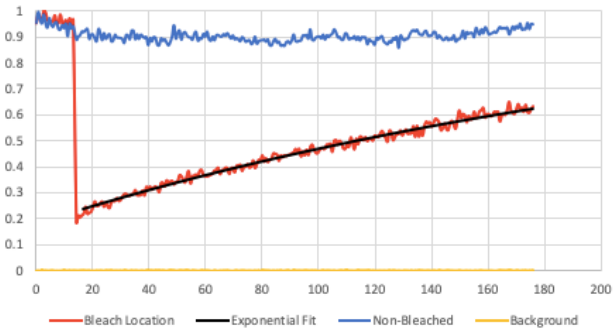

Figure 12. FRAP analysis. Fluorescein-labeled reflectin was assembled to ca. 1 micrometer diam. (pH 4.3, 100 mM NaCl, photobleached and scanned for fluorescence recovery in the laser confocal microscope (red trace). Blue = relative fluorescence of unbleached assembly; yellow = background fluorescence. X-axis =relative fluorescence; y-axis = time (sec).

FRAP analyses (e.g., **Figure 12**) show recovery of fluorescence after photobleaching of a small zone within a reflectin assembly labeled with fluorescein, on a time scale comparable to that of other proteins identified as LLPS droplets (71). FRAP analyses in which one-half of the fluorescein-labeled reflectin droplets were bleached showed the bleached sections to recover extensively over an average of 65 sec. Because the confocal microscope permits complete z-section analysis, confirming total bleaching of all of the fluorescein-reflectin in the volume irradiated by the high energy laser, and the photobleaching is irreversible, the observed recovery indicates relatively rapid diffusion of fluorescent reflectin molecules into the bleached volume, indicative of liquidity, either from other, non-bleached regions of the assembly, from other neighboring assemblies, or from the very low-concentration of unassembled monomers in the background.

Liquidity of reflectin assemblies also was convincingly evidenced by the observed fusion of fluorescein-labeled reflectin droplets, as seen in F**igure 13A.** Independently, fusion of reflectin assembly droplets also was observed by TEM (**Figure 13B.)**

As noted in section *g,* above, reflectin contains an unusually high content of aromatic (tyrosine) residues with remarkably regular periodicity across the entire protein (11, 15, 17), a feature recently identified as a strong determinant of protein liquid phase behavior (e.g., 36, 45).

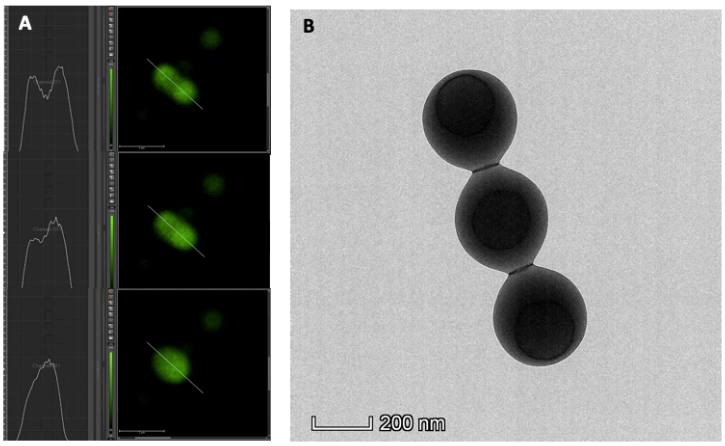

Figure 13A. Fusion of two fluorescein-labeled reflectin assembly droplets (ca. 1,000 nm diam. each). Fluorescent images taken ca. 20 sec. apart (from top to bottom), with cross-sectional scans of fluorescence intensity (indicated by white lines in fluorescent images) confirming fusion.

(**B**) TEM showing early stage of fusion of three reflectin assembly droplets (ca. 200 nm diam. each),

l. Reflectin can be used as a carrier to assemble other proteins:

As proof of principle for our proposed follow-on studies with amylin or the Tau-derived K18, we successfully used reflectin as a carrier for the tunably controlled, calibrated assembly of mCherry, a genetically engineered, red-fluorescing variant for the Green Fluorescent Protein. Using methods in daily use in our lab, and described below, we first genetically coupled mCherry to both the amino- and carboxy-terminal ends of reflectin A1, purifying the resulting chimeric proteins as inclusion bodies after expression in *E. coli.* Of these new recombinant proteins, the N-terminal adduct proved most useful, with the mCherry moiety refolding normally (after solubilization and chromatographic purification in urea), to reconstitute its red fluorescent core while assembling as part of the chimera, with assembly sizes progressively increasing with increasing pH (**Figure 14).**

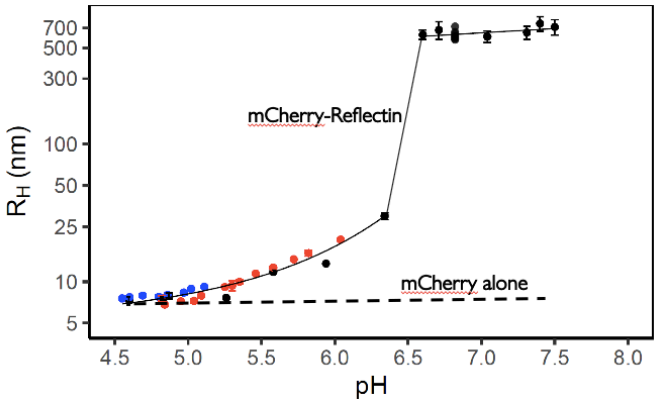

Figure 14. Tunably controlled, calibrated assembly of mCherry-Reflectin chimeric protein, as measured by DLS. Buffers (25 mM) were Na acetate (blue), MES (red), MOPS (black). Control showed no assembly of mCherry alone (points omitted for clarity).

E. References:

1. Izumi, M., A. M. Sweeney, D. G. DeMartini, J. C. Weaver, M. L. Powers, A.R. Tao, T. V. Silvas, R. M. Kramer, W. J. Crookes-Goodson, L. M. Mäthger, R. R. Naik, R. T. Hanlon and D. E. Morse. 2010. Changes in reflectin protein phosphorylation are associated with dynamic iridescence in squid. J. Royal Soc. Interface 7: 549-560.
2. Tao, A.R., D. G. DeMartini, M. Izumi, A. M. Sweeney, A.L. Holt and D. E. Morse. 2010. The role of protein assembly in dynamically tunable bio-optical tissues. Biomaterials 31:793-801.

3. Holt, A., A. Sweeney, S. Johnsen and D.E. Morse. 2011. A highly-distributed Bragg stack with unique geometry provides effective camouflage for Loliginid squid eyes. J. Royal Soc. Interface 8: 1386-99.
4. DeMartini, D.G., D.V. Krogstad and D. E. Morse. 2013. Membrane invaginations facilitate reversible water flux driving tunable iridescence in a dynamic biophotonic system. Proc. Natl. Acad. Sci. USA 110: 2552-2556; DO:I 10.1073/pnas.1217260110
5. Ghoshal, A., D. G. DeMartini, E. Eck, and D.E. Morse. 2013. Optical Parameters of the Tunable Bragg Reflectors in Squid. J. R. Soc. Interface 10: DOI: 10.1098/rsif.2013.0386.
6. DeMartini, D.G., A. Ghoshal, E. Pandolfi, A. Weaver, M. Baum, D. Morse. 2013. Dynamic biophotonics: Female squid exhibit Tunable Leucophores and Iridocytes. J. Exper. Biol. 216: 3733-3741.
7. Ghoshal, A. D.G. DeMartini, E. Eck and D. E. Morse. 2014. Experimental determination of refractive index of condensed reflectins in squid iridocytes. J. R. Soc. Interface 11: 20140106; http://dx.doi.org/10.1098/rsif.2014.0106
8. Holt, A.L., S. Vahidinia, Y. Gagnon, D. E. Morse and A. M. Sweeney. 2014. Photosymbiotic giant clams are transformers of solar flux. J.R.Soc. Interface 11: 20140678; http://dx.doi.org/10.1098/rsif.2014.0678 - plus cover.
9. Rotstein, R. S. Mitragotri, M. Moskovits and D. E. Morse. 2014. Progressive transition from resonant to diffuse reflection in anisotropic colloidal films. J. Polymer Sci. B: Polymer Physics 52: 611-617.
10. DeMartini, D. G., M. Izumi, A. T. Weaver, E. Pandolfi and D.E. Morse. 2015. Structures, organization and function of reflectin proteins in dynamically tunable reflective cells J. Biol. Chem. doi/10.1074/jbc.M115.638254
11. Levenson, R., C. Bracken, N. Bush and D.E. Morse. 2016. Cyclable condensation and hierarchical assembly of metastable reflectin proteins, the drivers of tunable biophotonics. J. Biol. Chem. 291: 4058-4068. DOI: 10.1074/jbc.M115.686014
12. Ghoshal, A., E. Eck, M. Gordon and D. E. Morse. 2016. Wavelength-specific forward scattering of light by Bragg-reflective iridocytes in giant clams. J.R.Soc. Interface 13: 20160285.
13. Levenson, R., D. DeMartini and D.E. Morse. 2017. Molecular mechanism of reflectin's tunable biophotonic control: Opportunities and limitations for new optoelectronics. Applied Physics Lett. – Materials 5, 104801: 1-12 [http://dx.doi.org/10.1063/1.4985758]
14. Morse, D.E. and S.,Johnsen, (Eds.). 2018. Bioinspiration and Biomimetics, Special Issue on Biophotonics and Biologically Inspired Photonics, 13: [https://doi.org/10.1088/ 051001-056006]
15. Levenson, R. C. Bracken, C. Sharma, J. Santos, C. Arata, B. Malady and D. E. Morse. 2019. Calibration between trigger and color: Neutralization of a genetically encoded Coulombic switch and dynamic arrest precisely tune reflectin assembly. J. Biol. Chem. 294: 16804-16815. doi: 10.1074/jbc.RA119.010339
16. Song, J., J. Santos, R.Levenson, L. Velazquez, F Zhang, D. Fygenson, W. Wu and D. E. Morse, 2020. Reflectin proteins drive fusion and remodeling of synthetic membrane vesicles. Langmuir (in press.)
17. Levenson, R., B. Malady, T. Lee, Y. Al Sabeh, P. Kohl, Y. Li and D.E. Morse, 2021 Protein charge Neutralization is the proximate driver dynamically tuning a nanoscale Bragg reflector. https://doi.org/10.1101/2021.04.23.441158
18. Hanlon, R. 2007. Cephalopod dynamic camouflage. Curr. Biol. **17**, R400–R404.

19. Hanlon, R. T. *et al.* 2009. Cephalopod dynamic camouflage: bridging the continuum between background matching and disruptive coloration. Philos. Trans. R. Soc. Lond*. B Biol. Sci.* **364**, 429–437.
20. Crookes, W. J. *et al.* 2004. Reflectins: the unusual proteins of squid reflective tissues. Science **303**, 235–238.
21. Cooper, K. M., Hanlon, R. T. & Budelmann, B. U. 1990. Physiological color change in squid iridophores. II. Ultrastructural mechanisms in *Lolliguncula brevis*. Cell Tissue Res*.* **259**, 15–24.
22. Cooper, K. M. & Hanlon, R. T., 1986. Correlation of iridescence with changes in iridophore platelet ultrastructure in the squid *Lolliguncula brevis* J. Exper Biol*.* 121: 451-455.
23. Vernon, R. M. *et al.* 2018. Pi-Pi contacts are an overlooked protein feature relevant to phase separation. eLife **7**, e31486.
24. Prilusky, J. *et al.* 2005. FoldIndex©: a simple tool to predict whether a given protein sequence is intrinsically unfolded. Bioinformatics **21**, 3435–3438.
25. Xue, B., Dunbrack, R. L., Williams, R. W., Dunker, A. K. & Uversky, V. N. 2010. PONDR-FIT: A meta-predictor of intrinsically disordered amino acids. Biochim. Biophys. Acta *BBA - Proteins Proteomics* 1804: 996–1010.
26. Kozlowski, L. P. & Bujnicki, J. M. 2012. MetaDisorder: a meta-server for the prediction of intrinsic disorder in proteins. BMC Bioinformatics **13**, 111.
27. Schneider, C. A., Rasband, W. S. & Eliceiri, K. W. 2012. NIH Image to ImageJ: 25 years of image analysis. Nature Methods. doi:10.1038/nmeth.2089.
28. Qin, G. *et al.* Recombinant reflectin-based optical materials. 2013. J. Polym. Sci. Part B Polym. Phys*.* **51**, 254–264..
29. Phan, L. *et al.* 2013. Reconfigurable infrared camouflage coatings from a cephalopod protein. Adv. Mater*.* 25: 5621–5625.
30. Naughton, K. L. *et al.* 2016. Self-assembly of the cephalopod protein reflectin. Adv. Mater. **28**, 8405–8412.
31. Guan, Z. *et al.* 2017. Origin of the reflectin gene and hierarchical assembly of its protein. Curr. Biol. **27**, 2833-2842.e6.
32. Thurlkill, R. L., Grimsley, G. R., Scholtz, J. M. & Pace, C. N. 2006. pK values of the ionizable groups of proteins. Protein Sci. **15**, 1214–1218.
33. Klein, R. & Von, G. H. H. 2001. Charge-stabilized colloidal suspensions. Phase behavior and effects of confinement. Pure Appl. Chem. **73**, 1705–1719
34. Hierrezuelo, J., Sadeghpour, A., Szilagyi, I., Vaccaro, A. & Borkovec, M. 2010. Electrostatic stabilization of charged colloidal particles with adsorbed polyelectrolytes of opposite charge. Langmuir **26**, 15109–1511.
35. Kyte, J. & Doolittle, R. F. 1982. A simple method for displaying the hydropathic character of a protein. J. Mol. Biol. **157**, 105–132.
36. Martin, E.W., et al. 2020. Valence and patterning of aromatic residues determine the phase behavior of prion-like proteins. Science 367: 694-699.
37. Choi, J.-M., A.S. Holehouse and R.V. Pappu, 2020. Physical principles underlying the complex biology of intracellular phase transitions. Ann. Rev. Biophys. 49: 107-133.
38. Shin, Y. and C.P. Brangwynne, 2017. Liquid phase condensation in cell physiology and disease. Science 357: (6357), eaaf4382. DOI: 10.1126/science.aaf 4382

39. Feng, Z., X. Chen, X. Wu and M. Zhang. 2019.Formation of biological condensates via phase separation: Characteristics, analytical methods, and physiological implications. J. Biol. Chem. 294: 14823–14835.
40. Wang, J., et al. 2018. A molecular grammar governing the driving forces for phase separation of prion-like RNA binding proteins. Cell 174: 688-699.
41. Patel, A., et al. 2015. A liquid-to-solid phase transition of the ALS fusion protein, FUS accelerated by disease mutation. Cell 162: 1066-1077.
42. Schuster, B., et al., 2018. Controllable protein phase separation and modular recruitment to form responsive membraneless organelles. Nature Comms. 9: 2985. doi: 10.1038/s41467-018-05403-1
43. Woodruff, J.B., A.Y. Hyman and E. Boke. 2018. Organization and function of non-dynamic biomolecular condensates. Trends Biochem. Sci. 43: 81-94.
44. Dogra, P., A. Joshi, A. Majumdar and S. Mukhopadyhay, 2019. Intermolecular charge-transfer modulates liquid- liquid phase separation and liquid-to-solid maturation of an intrinsically disordered pH-responsive domain. J. Amer. Chem. Soc. DOI: 10.1021/jacs.9b10892
45. Gabryelczyk, B., et al. 2019. Hydrogen bond guidance and aromatic stacking drive liquid-liquid phase separation of intrinsically disordered histidine-rich peptides. Nature Comms. 10:5465; doi.org/10.1038/s41467-019-13469-8
46. Liu Y, Xi Y. 2019. Colloidal systems with a short-range attraction and long-range repulsion: phase diagrams, structures, and dynamics, Current Opinion in Colloid & Interface Science, https://doi.org/10.1016/j.cocis.2019.01.016.
47. Levy, Y. and J.N. Onuchic. 2006. Mechanisms of protein assembly: lessons from minimalist models. Acc Chem Res. 39(2):135-42.
48. Deserno, M. 2001. Rayleigh instability of charged droplets in the presence of counterions. Eur. Phys. J. E 6, 163–168.
49. Safinya, C., et al. 2011. Nanoscale assembly in biological systems. Adv Mater. 23(20): 10.1002/adma.201004647.
50. Jawerth, L.M., et al. (2018). Salt-dependent rheology and surface tension of protein condensates using optical traps. Phys. Rev. Lett. 121: 25810; DOI: 10.1103/PhysRevLett.121.25810
51. Jiao, J., Rebane, A. A., Ma, L., & Zhang, Y. 2017. Single molecule protein folding experiments using high-precision optical tweezers. Optical Tweezers: Methods and Protocols (Ed.: A. Gennerich; Springrer) 357-390.
52. Liang, S.P., R. Levenson, B. Malady, M.J. Gordon, D.E. Morse and L. Sepunaru. 2020. Electrochemical resolution of protonated histidine reduction and its drive of reflectin protein assembly. Nature (submitted).
53. NetPhos 3.1 (http://www.cbs.dtu.dk/services/NetPhos/)
54. https://www.phosphosite.org/proteinAction?id=5142074&showAllSites=true
55. Charge, S.B.P., E.J.P. deKoninh and A. Clark. 1995. Effect of pH and insulin on fibrillogenesis of islet amyloid polypeptide *in vitro.* Biochem. 34: 14588-14593.
56. Kayed, R., et al., 1999. Conformational transitions of islet amyloid polypeptide in amyloid formation *in vitro.* J. Mol. Biol. 287: 781-796.
57. Wiltzius, J.J.W., S.A. Sievers, M.R. Sawaya and D. Eisenberg, 2009. Atomic structures of IAPP (amylin) fusions suggest a mechanism for fibrillation and the role of insulin in the process. Protein Sci. 18: 1521-1530.

58. Wei, L., et al., 2010. The molecular basis of distinct aggregation pathways of islet amyloid polypeptide. J. Biol. Chem. 286: 6291-6300; DOI 10.1074/jbc.M110.166678
59. Marek, P.J., V. Patsalo, D.F. Green and D.P. Raleigh. 2012. Ionic effects on amyloid formation by amylin are a complicated interplay among Debye screening, ion selectivity and Hofmeister effects. Biochem. 51:8478-8490. doi/10.1021/bi300574r
60. Gao, M., et al. 2015. Modulation of human IAPP fibrillation: Co-solutes, crowders and chaperones. Phys. Chem. Chem. Phys. 17: 8338-8348.
61. Seeliger, J., K. Estel, N. Erwin and R. Winter 2013. Cosolvent effects on the fibrillation reaction of human IAPP. Phys. Chem. Chem. Phys 15: 8902 -8907.
62. Birol, M., S. Kumar, E. Rhoades and A.D. Miranker. 2018. Conformational switching within dynamic oligomers underpins toxic gain-of-function by diabetes-associated amyloid. Nature Comms., 9: 1312-1322; doi: 10.1038/s41467-018-03651-9
63. Buee, L., et al., 2000. Tau protein isoforms, phosphorylation and role in neurodegenerative disorders. Brain Res. Revs. 33: 95-130. https://doi.org/10.1016/S0165-0173(00)00019-9
64. Wang, J.Z., Y.Y. Xia, I. Grundke-Iqbal and K. Iqbal. 2013. Abnormal hyperphosphorylation of Tau: Sites, regulation, and molecular mechanism of neurofibrillary degeneration. J Alzheimers Dis. 2013;33 Suppl 1:S123-39. DOI: 10.3233/JAD-2012-129031
65. Wang, Y., et al. 2012. Phosphorylated alpha-synuclein in Parkinson's disease. Sci. Trans. Med. 4(121): 121ra20. doi: 10.1126/scitranslmed.3002566
66. Gibson DG, Young L, Chuang, R-Y, Venter JC, Hutchison III CA, Smith HO. 2009. Enzymatic assembly of DNA molecules up to several hundred kilobases. Nature Meth.: 343-345.
67. Eisenberg, D., Weiss, R. M., and Terwilliger, T. C. 1982. The helical hydrophobic moment: a measure of the amphiphilicity of a helix. Nature 299: 371–374.
68. Eisenberg, D., R.M. Weiss and T.C. Terwilliger. 1984. The hydrophobic moment detects periodicity in protein hydrophobicity. Proc. Natl. Acad Sci. 81: 140-144.
69. Kozlowski, L. P. & Bujnicki, J. M. 2012. MetaDisorder: a meta-server for the prediction of intrinsic disorder in proteins. BMC Bioinformatics 13: 111.
70. Ilavsky, J. 2012. Nika: software for two-dimensional data reduction. J. Appl. Crystallogr. 45**:** 324–328.
71. Hirai, M. S. Arai, H. Iwase and T. Takizawa. 1998. Small-angle X-ray scattering and calorimetric studies of thermal conformational change of lysozyme depending on pH. J. Phys. Chem. B 102:1308-1303.